Design of millimetre wave components for additive manufacturing fabrication

Grado en Ingeniería en Tecnologías de Telecomunicación

Trabajo Fin de Grado

Joseph Zandueta Villanueva

Iván Arregui Padilla

Pamplona, 10 de junio de 2021

upna

Universidad Pública de Navarra
Nafarroako Unibertsitate Publikoa

AKNOWLEDGEMENTS

Firstly, I would like to express gratitude to my professor Iván Arregui who not just helped me anytime I needed but moreover he gave me clear advices and ideas about the next step to try when I was stuck at some stage of this process.

I could not recognise also David Santiago because he has been very helpful turning his chair to me every time I asked him. He offered selflessly many concepts regarding day-to-day and theoretical notions.

Lastly, I also would like to thank Marcelo who encouraged me to study this degree back in 2017.

CONTENTS

1.   INTRODUCTION

1.1   KEY WORDS

3-D printing, additive manufacturing, band pass filters, cavity resonator, Chebyshev filters, coupling coefficient, coupling matrix, external Q, gap waveguide, groove gap waveguide, artificial magnetic conductor, microwave filter, millimetre wave, mutual coupling, nails, periodic structures, rectangular waveguide, resonator filter, selective laser melting, scalmalloy, transmission zero, waveguide.

1.2   BACKGROUND

Telecommunications are the present and future of this modern world.

Since the discovery of Maxwell's formula in 1865 we have advanced a lot in the enduring path of controlling and communicating through microwaves. Barrow and Southworth published in 1936 the first evidence of transmission through a waveguide [1] and three years before Schelkunoff and Mead determined the existence of the today known as TE_{10} mode with an attenuation factor inversely proportional to the frequency [2].

At this moment the radiofrequency (RF) spectrum is saturated. Microwaves are used in vast applications from health to radio-communication. Everything that's here (Wi-Fi, cellular network, RFID[1]...) takes up on the familiar spectrum, up to 5 GHz.

Thus, with a future perspective we require to develop devices working at higher frequency bands like New Radio (NR) already does. This field is what we call millimetre waves (mm-waves), going from 30 GHz until the so-called terahertz at 300 GHz. Depending of the use we need and perks of each frequency we will use guided means like waveguides or free air solutions like antennas.

Waveguides are just a metal structure filled with a dielectric such as air or vacuum who are able to propagate different shapes of electromagnetic field along its axis. Advantages like the small insertion losses (IL), they are capable of deliver big amounts of energy with the benefit of small dispersion delay and they are easy to make are some of the reasons of why are used in high (HF) applications. However, in order to fulfil the current world's needs of increasing data rate as well as benefit from phenomenon like the ionosphere's transparency at super high frequencies (SHF[2]) we have reached frequencies where start to appear problems regarding surfaces refinement or edges affecting the overall response.

In order to obtain waveguides able to work above 30 GHz, gap waveguides (GW) were presented in 2009 [3] bringing a solution to manufacturing problems. There several variations, being groove gap waveguides (GGW) the chosen in this work.

---

(1)   *Radio Frequency Identification (RFID) is a passive wireless communication.*
(2)   *Frequency range for SHF is between 3 and 30 GHz.*

As depicted in Fig. 1, GGW consists in a regular hollow waveguide surrounded not by a regular wall but a series of metal pins (also called nails).
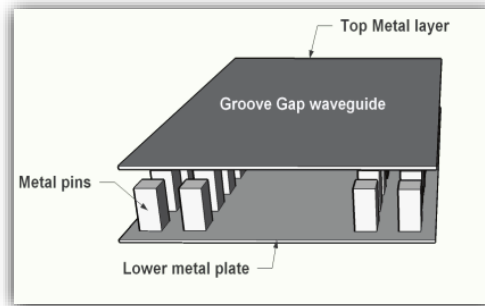

Figure 1: Geometry of groove gap waveguide [4]

They have two distinctive settings: the distance between the top of the pin and the upper plate must be less than quarter-wavelength ($\lambda/4$) of the frequency we want to avoid propagation and so also should be the length of the pin, from bottom to top.

Their structure of bed of nails beside the propagation axis simulates a wall to electromagnetic waves confining the electric field inside the waveguide aperture. At the same time, it eases alignment between pieces and fabrication with traditional methods like milling, because as not physical contact is needed imperfections can be obliterated.

Fabrication is another key aspect. At this point the accuracy we need is about quarters of millimetre in order to reproduce the desired behaviour of inverters or inductances within waveguides. Traditional milling processes consists in a small drill bit making its way through the metal plate, which obviously must be thinner than the space we want to create. It's not difficult to imagine the forces we apply when milling small pins through this system and the fragility of itself. Because of this the resolution we are used to get is around 1 mm.

3D printing technologies, also known as additive manufacturing possibilities have revolved the mechanics and manufacturing and bring also a new perspective of designing waveguides.

Fused deposition modelling (FDM) is the most common method where plastic is fused into a small moving nozzle which shapes the desired form. It allows to create props, DIY projects, gadgets… whereas in Telecommunication field is stereolithography (SLA) the preferred one. In this case, a liquid resin is hardened thanks to ultraviolet (UV) light. Anyway, since this material is the easiest to operate with, plastic waveguides with metal coat were the first ones to be tested.

Although, printing on metal is a goal due the strength and durability, so techniques like selective laser melting (SLM) or direct laser sintering (DMLS) the ideal, see examples on Fig. 2.

With their respective differences, these processes revolve around a laser beam melting very small metal particles (dust). Studies analysing its structural differences can be found in [5] but a key point is the resolution, which decreases until 30 µm.

As for the materials, titanium has been the traditionally used in this kind of additive manufacturing with several commercial applications but in our field (RF) more light-weight materials are needed and aluminium proved to be suitable too.

Figure 2: 3D printed waveguides (SLM) [6].

Another important characteristic is the enhanced properties this technique brings. Out there are many composites specially developed for additive manufacturing. For example, Scalmalloy®, an aluminium-magnesium-scandium allow. Although aluminium differs from steel in its thermal conductivity, SLM-induced properties are similar when it's used [7].

In this approach, selective laser melting allows new kind of structures while maintains the mechanical characteristics but there are not many studies about the electromagnetic behaviour.

1.3   MOTIVATION

In the 1950s resonators with evanescent modes were first proposed where dielectric posts could affect to the cut-off frequency [8].

Nowadays this occurrence is well-documented and allows to decrease the length of waveguides with same performance and the existence of filters based on coupled resonators.

Selectivity is demanded every application and is not easy to achieve at high frequencies. In order to accomplish it, transmission-zeros (TZ) can be introduced in the passband.

We can build capacitive apertures or half-wavelength ($\lambda/2$) shunt waveguides to realize TZ on the higher side of the passband [9]. On the other hand, if we want to do so in the lower side we need cross-coupling and multimode cavities are suitable for this. Such waveguide filters are explained in [10].

The aspiration of this work is to design a bandpass filter along a GGW waveguide based on coupled resonators.

It's very interesting applying this know-how to design a filter using overmoded cavities so I will present the basis of that knowledge.

1.5   ITINERARY

This project supposed the first experience in different fields like CAD design of waveguide (which implies *connaisance* of the specific software CST®), remembering concepts regarding filters and of course learning brand new concepts about resonators, cavities and so on.

Besides that, theory about cross-coupling and transmission zeros is introduced, yet there is much room to learn about.

In order to make this project feasible, it was divided in several tasks. This report is classified upon that too.

In Chapter 2, regular and GGW waveguides will be presented as well as the strategic parameters to characterize the looked-for functioning.

In Chapter 3 this knowing will be applied to design a GGW coupled resonator waveguide filter. In this case there are two important factor who will help to describe a filter: coupling factor and input coupling. So as to improve efficiency, two Python programs were designed to make this job better.

In the final chapter, nature of overmoded cavities will be explained and a filter based on this will outline without losing the groove gap perspective.

2. WAVEGUIDE TECHNOLOGY

Waveguides are one of the earliest lines of transmission discovered. Rectangular or circular, consists in a hollow metallic tube, where air can flow along its axis or remains vacuum.
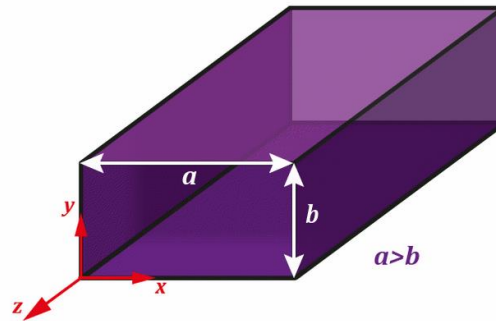

Figure 3: Dimensions of a rectangular waveguide [1].

As other electromagnetic devices, waveguide's operation lies on Maxwell's formula, which are extensively documented in several books [1] [11] .

Electromagnetic field can be expressed in any of the solutions of the wave equation. Along waveguides we can talk about TE and TM modes, where respectively the axial electric E_z or magnetic component H_z equals to zero. There is another mode called TEM where $E_z = H_z = 0$ but it needs two not-shorted conductors to propagate, what a waveguide doesn't comply with.

The key aspect is that we only need the axial components to solve the differential equation given the boundary conditions of the particular waveguide. In that case, we can obtain the propagation constant and wave impedance.

2.1 RECTANGULAR WAVEGUIDE

Waves are mathematically descripted in Euler's formula (1), and electromagnetic waves are no exception.

$$e^{jx} = \cos x + j \sin x \tag{1}$$

In this latter case, a sinusoid is defined by the constant propagation γ where α is what we call attenuation coefficient and β is the propagation constant, which represents the variation in phase per unit of length, measured in radians per meter (rad/m).

$$e^{jx} \rightarrow e^{\gamma} \tag{2}$$

$$\gamma = \alpha + j\beta \tag{3}$$

Another important coefficient is wavenumber k, the relation between angular frequency ω [rad/m] and speed of light c [m/s] (4)

$$k = \frac{\omega}{c} \tag{4}$$

Along rectangular waveguides we can find TM and TE modes. Although the expression of these fields is different we find the same way to obtain β (5).

This value is constrained by rectangular waveguide's geometry (Fig. 3), having also a cut-off frequency f_c given by (6), where ϵ_r is effective permittivity of the medium (1 in vacuum), μ_r is the magnetic permeability (1 in vacuum too), m, n are the conventional index for spatial distribution of electromagnetic fields. a, b are length and width of the waveguide, measured in units of International System of Units (IS).

$$\beta = \sqrt{k^2 - k_c{}^2} = \sqrt{k^2 - \left(\frac{m\pi}{a}\right)^2 - \left(\frac{n\pi}{b}\right)^2} \tag{5}$$

$$f_{c_{mn}} = \frac{c}{2\pi\sqrt{\mu_r\epsilon_r}} \sqrt{\left(\frac{m\pi}{a}\right)^2 + \left(\frac{n\pi}{b}\right)^2} \tag{6}$$

Thus, the behaviour and frequency will rely mainly on the waveguide's dimensions and they will be the same no matter whether it's the TE or TM which propagates.
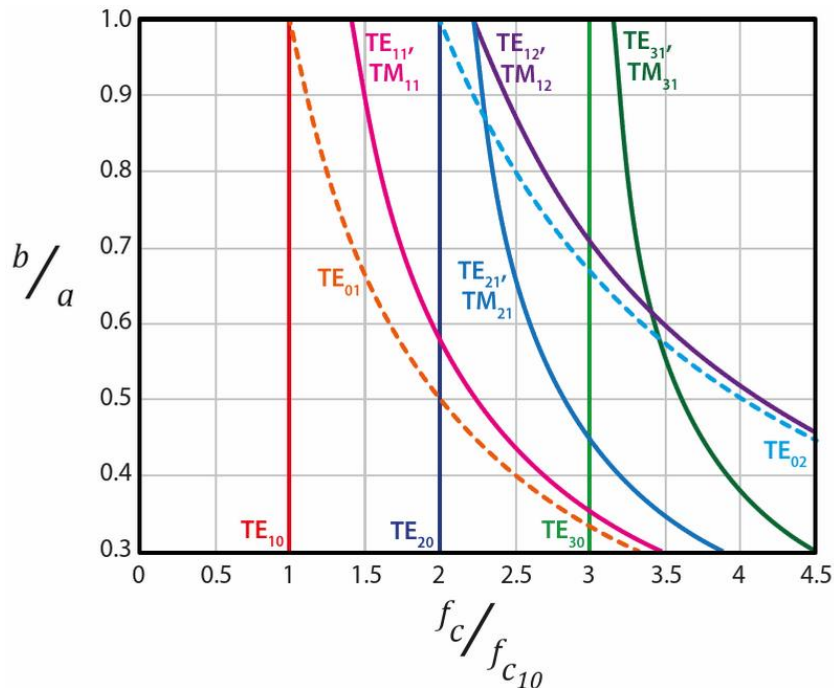

Figure 4: Relationship between shape, cut-off frequency and mode [1].

TE_{10} is the dominant mode with lowest cut-off frequency. As we can see in Fig. 4 that's the first mode that propagates along the guide (by convention it could be the z axis). The next mode doesn't start to propagate until frequency doubles.

As modes as just a physical distribution of the electromagnetic field, we try to get a single one in order to ease the work with it. That's what we call single-mode, the following ones would be a sum of the modes with higher cut-off frequency (Fig. 5)

As we try to get the widest bandwidth possible as well as not entering into multi-mode, best relation between width and height is $\frac{b}{a} < 0.5$ because then the frequency span until next mode arrives is the biggest possible and also then TE_{20} would appear before any other mode.

In the end, the chosen relation is 0.5, because allows the maximum amount of power as it depends on the section surface, $S = ab = 0{,}5a^2$.
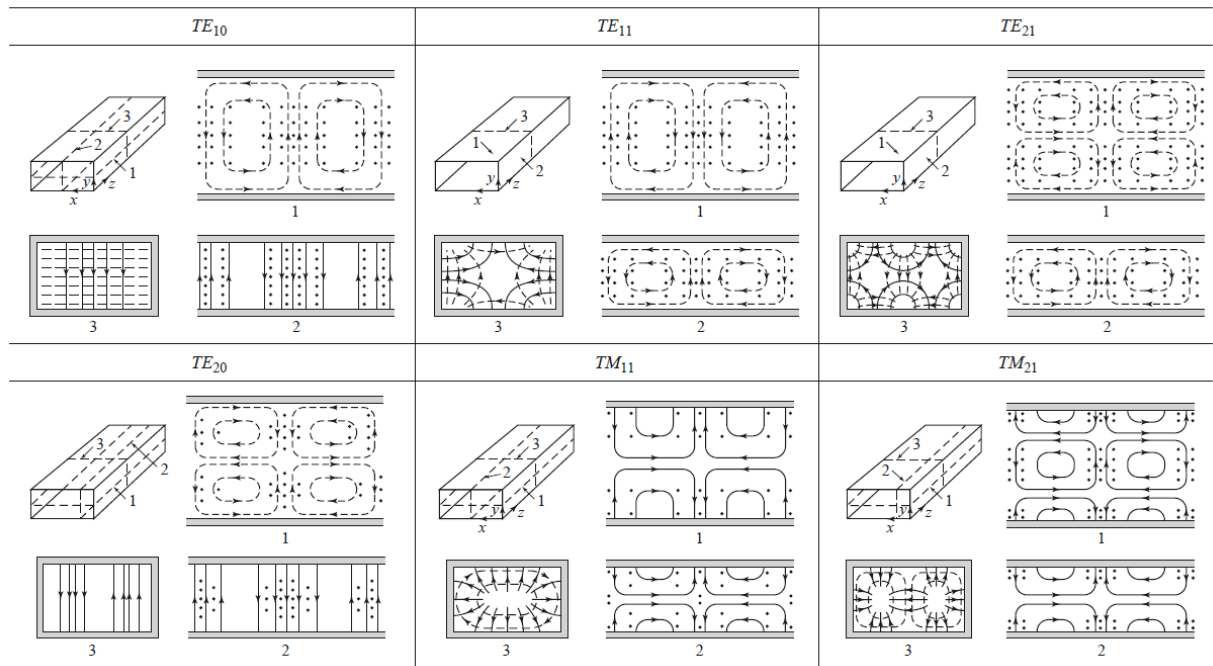

Figure 5: Field's spatial representation within rectangular waveguides [11].

The reason of using waveguides despite the bulky they are is because the little insertion losses (IL) they suffer, coefficient that is inverse proportional to the frequency, so it's used for high frequency (HF) appliances. The other advantage is the amount of power they can deliver if we compare to wires.

The problem of increasing frequency is the shortening wavelength, making physical imperfections "visible" to the wave. Also, the way of manufacturing implies dividing the piece in two halves. This edge provokes high return losses (RL) and reflections.

That's why engineers deliberated type of waveguides able to go over these problems, discovering the gap waveguides.

2.2   GAP WAVEGUIDE

Gap waveguides appeared to solve some of the problems that regular waveguides suffered when increasing the frequency above 30 GHz. They could be seen as the evolution of a substrate integrated waveguide (SIW).

This device consists in two parallel plates with a substrate between them (Fig. 6). Artificial waveguides are constructed by inserting via holes acting as walls, but there were loss due the substrate [12].
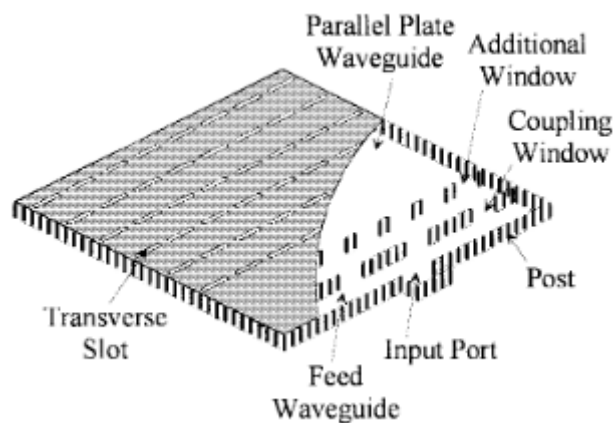

Figure 6: Scheme of SIW [9].

Gap waveguides are based on a perfect electrical conductor (PEC) plate in front of an artificial magnetic conductor (AMC). We find in several papers notation like hard/soft surfaces, but they are portrayed from Acoustics because of the similar behaviour and are not accurate. They aim to describe surfaces where propagation is allow in certain angle, normally along propagation while not in other (transverse direction).

We can build an AMC as a corrugated surface made of a perfect electric conductor (PEC) where the groove depth is $d = \left(\frac{\lambda}{4}\right)$. At the bottom of the it we have a short-circuit given by the PEC nature. However, the distance between the strips makes an open-circuit at the top of the strips. As I will explain later, this design turned into a bed of metal pins (Fig. 7).
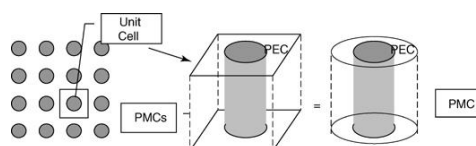

Figure 7: Equivalent unit cell for medium [13].

Over an AMC transverse magnetic component H_t=0, which turns into a surface where waves can propagate along the strips but decreases in any other direction, whereas they stop orthogonally

to them. This effect will only occur when it's set a gap with length $h = \left(\frac{\lambda}{4}\right)$ between these two plates, so the wave is attenuated in the transverse direction. [14]

Therefore, waves in the gap between this PEC/AMC surface can propagate along the PEC strips but are in cut-off for any other direction. More precisely, we would avoid TM_{mn} and TE_{mn} propagation when the gap is defined by $h \leq \left(\frac{\lambda}{4}\right)$.

As usual, the geometry determines the performance. In gap waveguides, the bandgap starts from the frequency at which groove depth is λ/4. The upper frequency is limited by $d + h = \frac{\lambda}{2}$. (Fig. 9)

Currently, the corrugated surface is replaced by a bed of nails, compelling the high impedance boundaries while allowing not only straight paths in the propagation direction. At any case, they both can be seen as a frequency selective surfaces (FSS).

Unlike conventional waveguides, there is no need of contact between the plates because of the stated boundary conditions confines the waves along the guide path. This is very useful because it relieves manufacturing processes. Also, this technology would allow to achieve a contactless flange adapter for waveguides. [15]

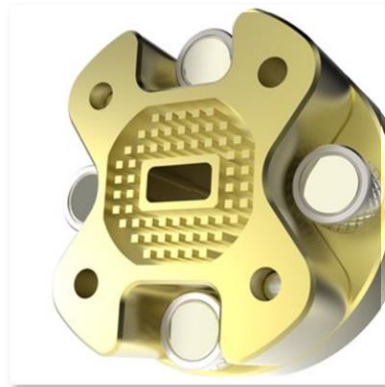This is very useful to simplify connection with waveguides reducing RL (Fig. 8)

Figure 8: Contactless flange adapter [16].

To sum up, the reasons behind GW are used are:

- They simplify alignment.
- The fabrication becomes easier.
- **It improves performance at HF.**

As for metal pins design, it doesn't matter if they are cylinders or squares (Fig. 9). There are thesis and studies analysing this and different parameters related to bandgap and how they behave., so it's not necessary to re-do any of those [17].

Best values for pins' dimension are applied following the following rules.

2.2.1 DESIGN OF METAL PINS

The purpose of metal pins is creating a space where electromagnetic waves are attenuated in any direction, leaving the waveguide aperture as the main path where they can propagate.

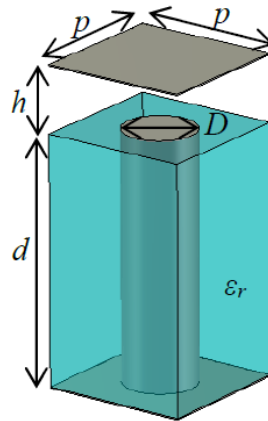The pins construction must consider several aspects:

Figure 9: Periodic unit cell [17].

- **Height of metal pins** → Reiterating, pins should be as long as quarter-wavelength of the beginning of the bandgap ($d = \lambda/4$) and it will end when gap + height equals half-wavelength ($h + d = \lambda/2$).
- **Relation between diameter *D* and height *d*** → This feature is not as important as the previous one, since having a ratio $d/D = 2$ will have similar results (in terms of bandgap) to $d/D = 5$
- **Relation between diameter *D* and periodicity p** → Periodicity means the space occupied by the pin and the space surrounded until next pin element. This defines a bit more the performance. A good bandgap happens until we apply $p/D = 3$ and from that it decreases gradually. Then, when we design metal pins in GW it's desirable to have a distance between pins lesser than the side of itself, e.g. 85-90% (7).

$$\frac{(2*0,9+1)*D}{D} \leq 3 \qquad\qquad (7)$$

2.2.2   TYPES OF GAP WAVEGUIDES

Starting from the basic structure of metal pins, other type of structures can be realized.

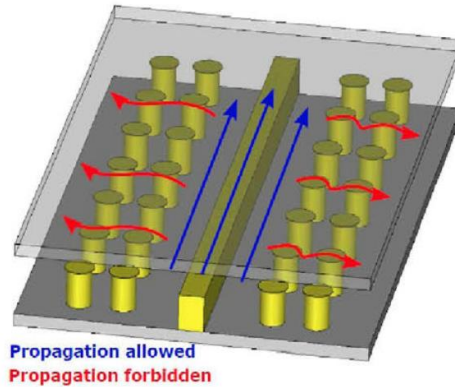Ridge gap waveguide have a metal elevation where electrical field propagates (Fig. 10) while

Figure 10: Ridge gap structure [18].

groove gap waveguides eliminate this element having a clear waveguide aperture.

In this work, groove gap waveguide was decided because it has several advantages despite of the main disadvantage (e.g. compared to microstrip) that is bulkiness.

- They can be mass producible.
- There is not any electrical contact, while devices like SIW need that. RGW needs a circuit made on same metal coat too.
- They have low losses. SIW brings losses related to dielectric and RGW because of ohmic losses.

2.2.3   DESIGN OF A GGW

A WR22 waveguide is designed with groove gap technology . In this case of study, the waveguide is planned to work along another waveguide, connected by flanges. Waveguides with coaxial connections won't be studied in this work.

22 stands for 220 mils wide, a = 5.6896 mm in IS. The height, follows the rule $\frac{b}{a} < 0.5$ and it is the half: b = 2.8448 mm (Fig. 11).

The frequency range is typically 33 - 50 GHz, even though the lowest propagating frequency is 26 GHz.
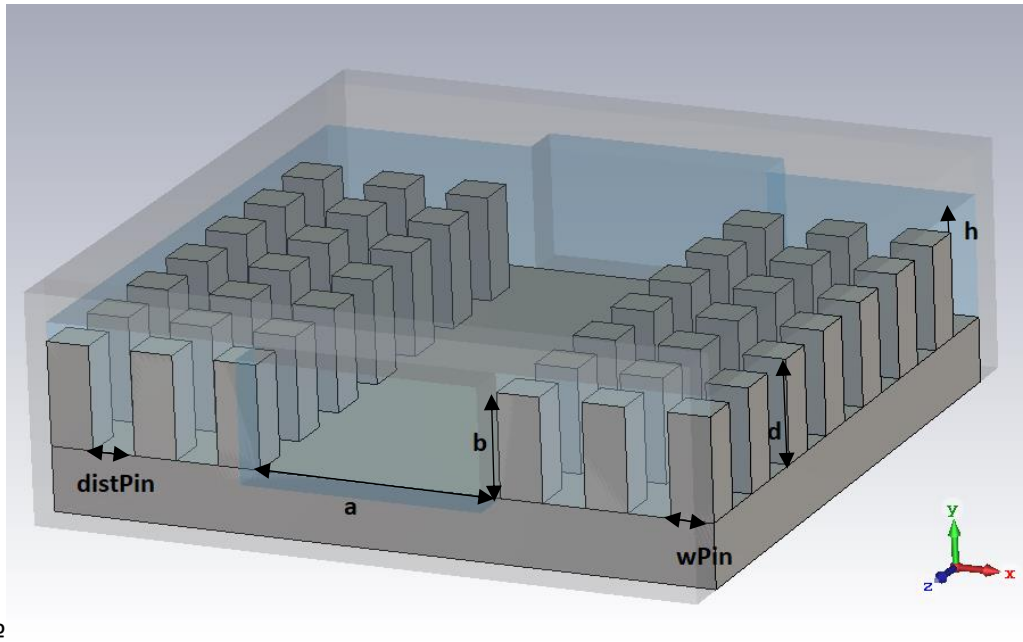
º

Figure 11: Design of 3-rows GGW.

Basic structure is shown on Fig.11. Three lines of metallic pins are set, where each of them is d = 2.27 mm long. This height was chosen attending to the desired frequency we would like to start the bandgap f_{min} = 36 GHz.

The pins are $wPin$ = 0.9 mm each side then distance between them $distPin$ = 0.8 mm (7)

Gap between the top of the pins and the upper plate in this case is h = 0.445 mm.

TABLE I: Dimensions of GGW WR22	
Parameter	**Value [mm]**
a	5.6896
b	2.8448
d	2.27
wPin	0.9
distPin	0.8
h	0.445

A proper S parameters graph is obtained, verifying the correct performance of this technology.

Electric field radiated further than the second row of pines is very low, about 40 dB lower than the current flowing across the waveguide aperture.

Considering this, a GGW with just only two rows of pins is tested.

In Fig. 12 can be seen the electric field radiated in two cases (3 and 2 rows of pins) as well as the exact same performance in terms of scattering parameters, as expected.

There should be measured with an open-space boundary to have a better view of the fields "radiated" out of the waveguide.
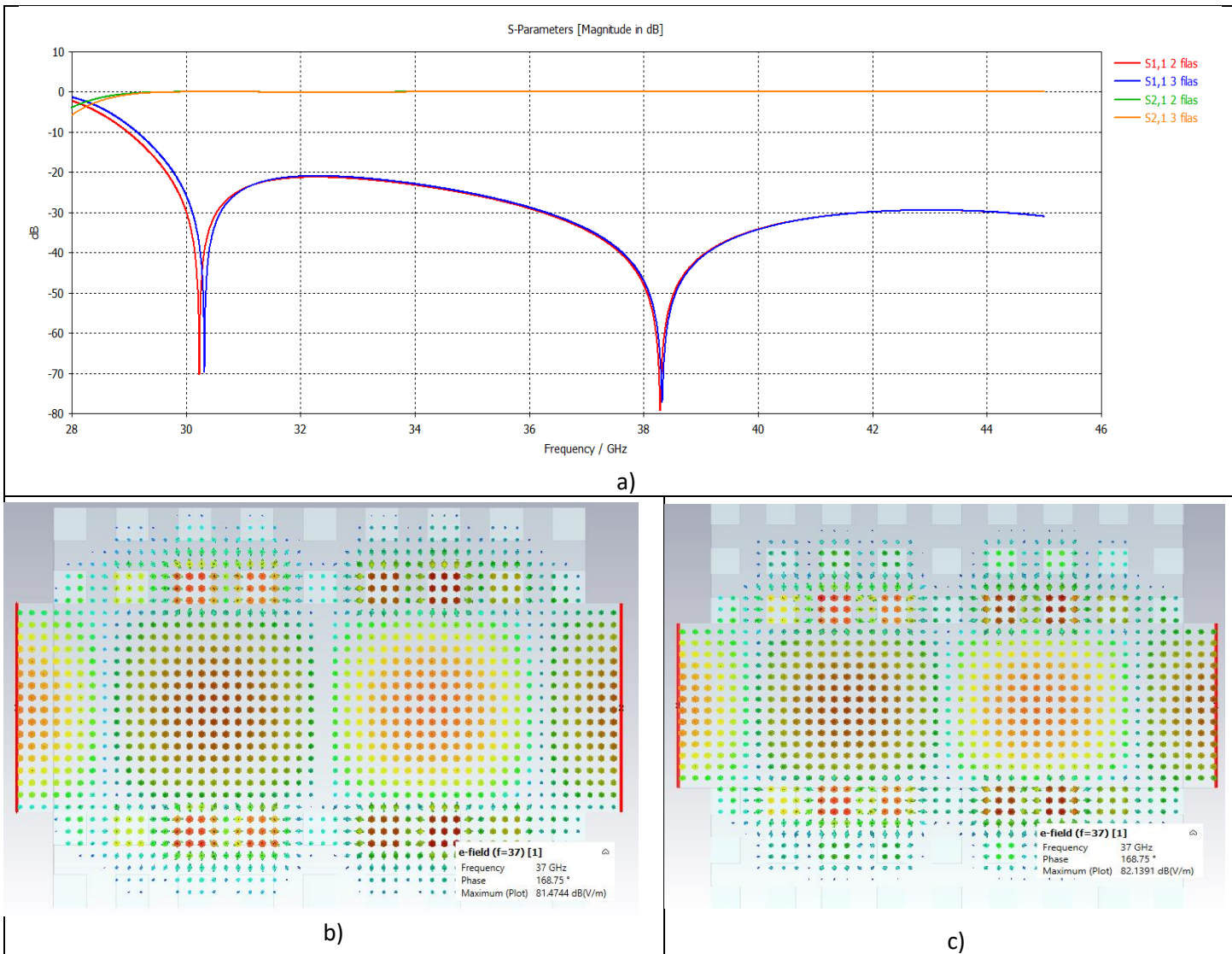
Figure 12: a) Dual response, b) electric field at 2D view with two rows and c) three rows.

It's confirmed that GGW technology is as good as regular hollow waveguides to transport microwaves, reflecting up to -20 dB in the worst case.

2.2.4 ADDITIVE MANUFACTURING (SLM) FOR GGW

Scalmalloy® is an aluminium-magnesium-scandium (AL-Mg-Sc) allow patented by Airbus APWorks envisioned for aerospace applications thanks to its light-weight while retaining excellent mechanical characteristics.

This SLM process consists in introducing the Scalmalloy® powder into a N_2 controlled atmosphere to be melted with a laser. Temperature must be precisely before fusion point and must be meticulous to prevent from cracking, as well as it should hold gradually afterwards for same reason, what is called ageing [19].

This technique permits 30 μm slice thickness and print speed is around 22 cm^3 per hour, reaching a density around 99% [20].

Also, it achieves one of the best mechanical properties relating to elongation and offset yield strength (Fig. 13).
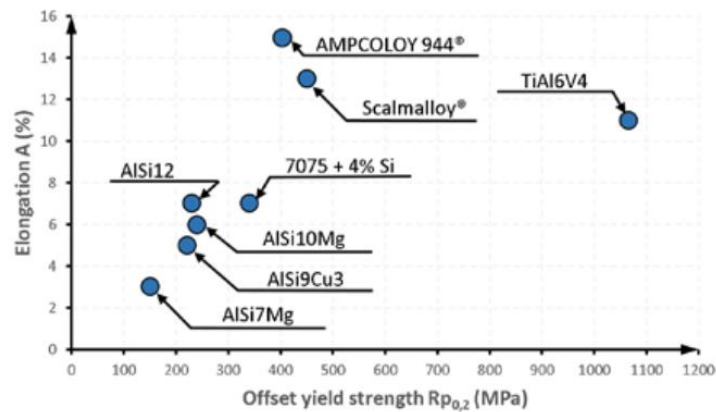

Figure 13: Comparison to other materials in SLM [20].

As I mentioned before, there are not literature about the possibilities that this material could contribute to RF.

In the eagerness to discover it, a GGW model whose functionality was already proven after traditional fabrication (milling) was used to 3D print it (Fig 14).
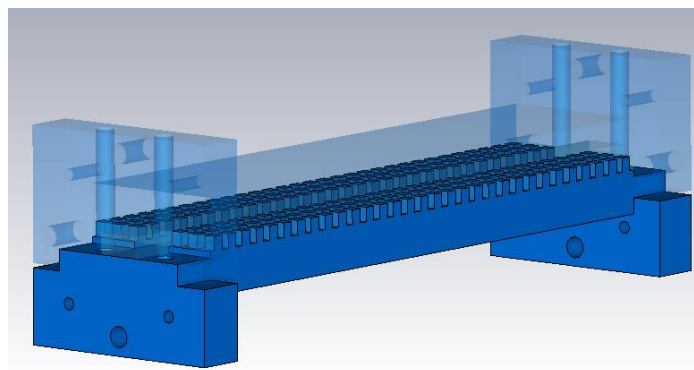

Figure 14: Model of WR22 GGW.

Particularly it was sent a WR22 waveguide. Exact dimensions can be seen in Table 2.

TABLE II	
Parameter	Value [mm]
a	5.6896
b	2.8448
d	2.745
wPin	1.56
distPin	1.23
h	0.1

It was split in two halves and send to fabricate to a company (Labcyp) in Cádiz.

At the moment of writing this work the waveguide was still under post-processing and it wasn't possible to analyse it (Fig. 15).
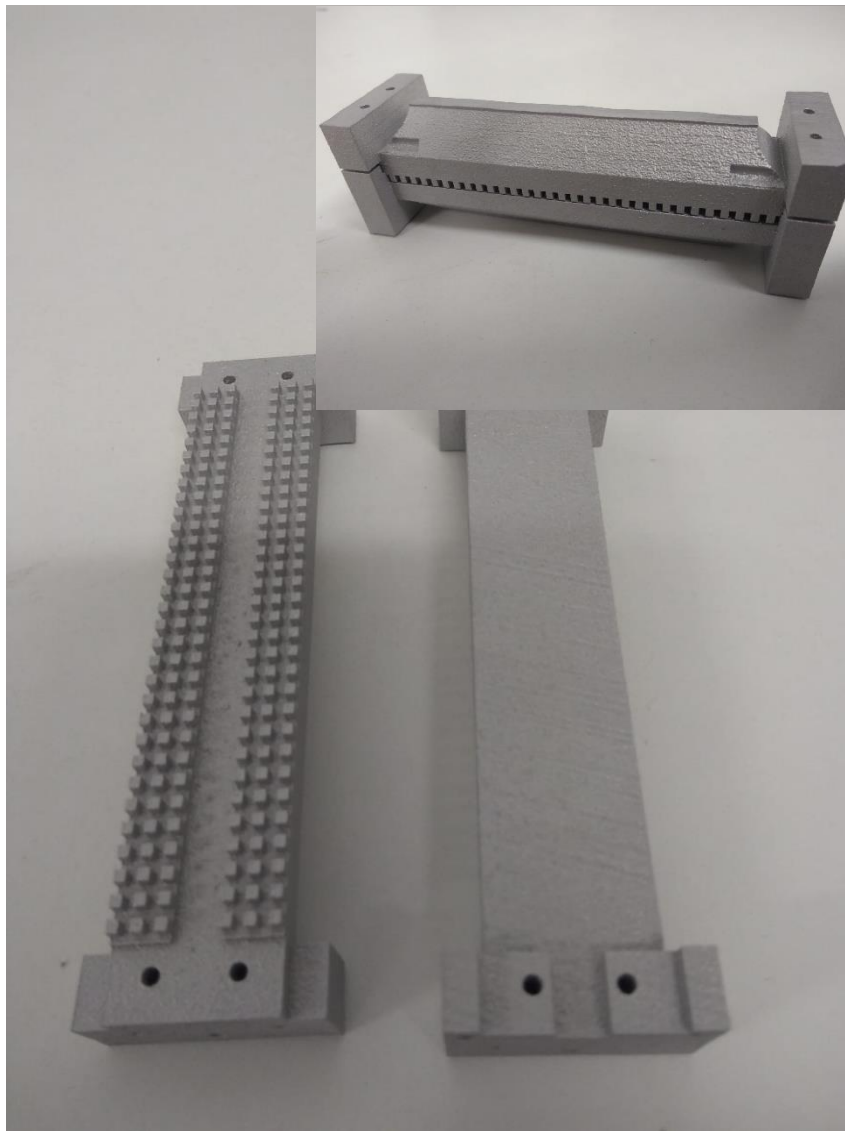

Figure 15: View of the WR22 SLM GGW

3.   COUPLED RESONATORS WAVEGUIDE FILTERS

3.1   DESIGN APPROACH

A filter is a selective frequency device able to discriminate between the whole bandwidth depending on the goal we want to achieve. For example, given the range of operation possible for a WR22 waveguide, they can limit the power delivered to a load, like an antenna.

Creating adapted systems is crucial and filters play an important role along other devices (e.g. matching networks), being an essential part of engineering and communication systems. They can be designed based on different technologies.

The simplest type of filter comes as the lumped-elements model known as RLC resonant circuit, whose impedance is as follows:

$$Z_{\text{in}} = R + j\omega L - j\frac{1}{\omega C} \tag{8}$$

It's trivial to deduce there will be a point where impedance will be strictly real, what we call resonance. Impedance will be at its lowest and delivered power will be maximum (Fig. 16).
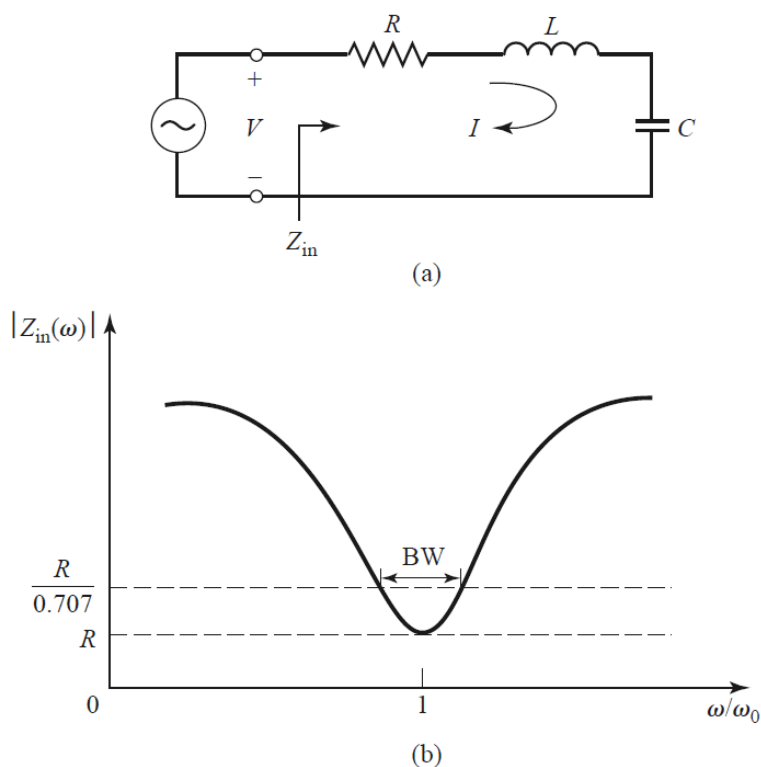

Figure 16: Series RLC and its response [11].

When microwaves frequencies are beyond lumped-elements' reach, distributed elements are used. We know the basis of this behaviour is $\frac{\lambda}{2}$ means within shorted transmission lines at both ends and microwave resonators are no exception.

Thus, cavities ought to be an integer multiple of this length at the desired frequency, which it's ruled by (9).

$$f_{mnl} = \frac{c}{2\pi\sqrt{\mu_r\epsilon_r}}\sqrt{\left(\frac{m\,\pi}{a}\right)^2 + \left(\frac{n\,\pi}{b}\right)^2 + \left(\frac{l\,\pi}{l}\right)^2} \qquad (9)$$

According to this formula, it's possible to calculate the frequency at which there will be a resonance depending on resonator length l and verify it with CST Eigenmode Solver.

However, when narrow-band filters are required is not enough with the natural resonance and coupled resonators filters are needed. In this case, inductances, capacitances and resistance of each resonator disturb the adjacent ones creating mutual impedances and what we call coupling coefficient K_{ij}. These values determine the filter specification: fractional bandwidth Δ, return losses RL, central frequency f_0; they normally come in the shape of matrix.

This model of designing filters is widely used because is useful regardless technology used and can be found in any electromagnetic suite like CST® or ADS®

If we want to design a filter we should take note of the specifications already mentioned and introduce them into the Filter designer, getting a matrix of values we will look in detail (Fig. 17)
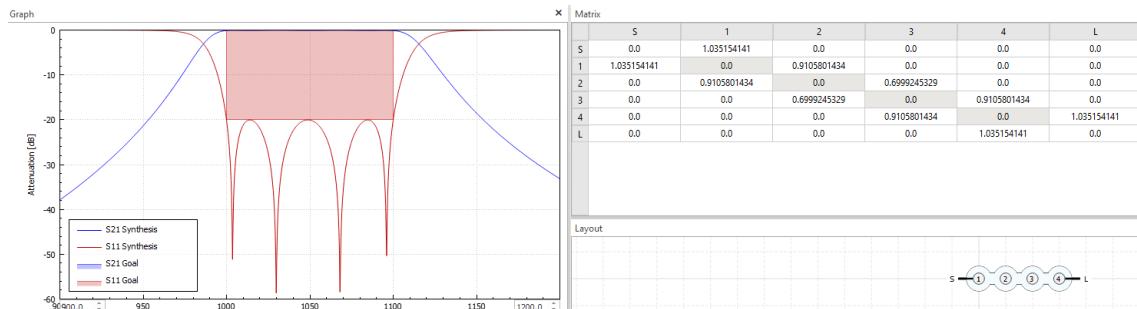

Figure 17: CST Filter designer

There is literature about procedure to design these type of filters [21], so it will be followed to design a GGW filter and prove the equivalent performance as a regular waveguide filter.

3.2   WR22 COUPLED RESONATOR FILTER (GGW)

In order to achieve a Chebyshev filter based on gap technology, requirements of a known 5th order filter are chosen.

The specifications of the filter are:

TABLE III: 5th ORDER CHEBYSHEV FILTER	
Bandwidth [f_{min} - f_{max}]	[36.5 – 38] GHz
Central frequency [f_0]	37.3 GHz
Return losses [RL]	20 dB

RL is directly connected to the ripple ϵ, 20 dB of return losses will result in a 0.1 dB ripple.

$$\epsilon = \frac{1}{\sqrt{10^{\frac{RL}{10}}-1}} \qquad (10)$$

Firstly, to calculate the values it should have. Expanding the Chebyshev polynomials for low-pass model gets the following g_i values:

g_0	g_1	g_3	g_4	g_5	g_6
1	0.973228	1.37228	1.80319	1.37228	0.973228

These values determine the performance as a lowpass filter. They could be used for design a filter based on lumped elements and get the desired response.

Unfortunately, parasite impedance of these elements won't allow to do so at very high frequencies. Mathematically, bandpass transformation could be done to insert them into a simulation suite obtaining the filter response.

As I mentioned before, CST has a Filter designer that plots the response and matrix. When I introduced all specifications (Table 3) the program returned the next matrix:

0	1.013670655	0	0	0	0
1.013670655	0	0.8653188084	0	0	0
0	0.8653188084	0	0.6357125594	0	0
0	0	0.6357125594	0	0.6357125594	0
0	0	0	0.6357125594	0	0.8653188084	0
0	0	0	0	0.8653188084	0	1.013670655
0	0	0	0	0	1.013670655	0

Which clearly don't match with the g_i I mentioned before. This is because what CST does is plotting the M_{ij} matrix, skipping the bandpass transformation (11).

It's easy to compute the values and get exact same results. Important info that can be here is the relation between different elements are symmetric so the filter will be a reciprocal device.

Note that the coupling factor between the port and first resonator need a slightly different formula without square root, which it's called R_1.

$$M_{ij} = \frac{1}{\sqrt{g_i g_j}} \qquad (11)$$

$$R_1 = \frac{1}{g_i g_j} \qquad (12)$$

R_1	M_{12}	M_{23}	M_{34}	M_{45}	R_1
1.013	0.8653	0.6357	0.6357	0.8653	1.013

In this case, the formula I will use is the coupling factor between resonators, given by the relation between the fractional bandwidth Δ, also known as *FB,* and such values:

$$\Delta = \frac{BW}{f_0} \qquad (13)$$

$$K_{ij} = \frac{\Delta}{\sqrt{g_i g_j}} \qquad (14)$$

The fractional bandwidth is important because is the ratio between bandwidth (BW) and f_0, so even filters with similar response will need different measures depending on f_0.

Also, the input coupling (it's denoted also as external quality) of the filter depends on Δ:

$$Q_{\text{ext}} = \frac{1}{\Delta * R_1} = \frac{37.3}{1.5\,R_1} = 24.39 \qquad (15)$$

Getting the following series.

Q_{ext}	K_{12}	K_{23}	K_{34}	K_{45}	Q_{ext}
24.39	0.0347793	0.025551	0.025551	0.0347793	24.39

The length of the resonator determines f_0. In this case of study, it can be calculated with the help of software Mathematica and (9) so following Table 3 it needs to be l = 5,67 mm, value verified getting the eigenvalues. The rest of sizes are the same as in Table 1.

There are several ways to obtain coupling factor K_{ij} [21], which is inductive because of using a iris. In this case, I decided to calculate using the S parameters. Here what is examined is the resonance frequencies f of two same resonators separated by an iris with length p. Iris width is also *wPin*. Cavities must be weakly coupled so several metal pins are placed at the input/output ports (Fig. 18).
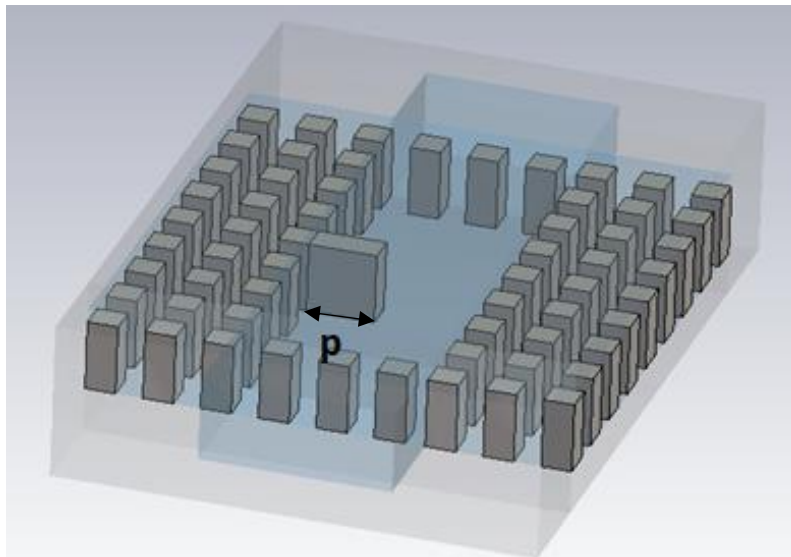

Figure 18: 3D view of the two resonators

Length of the iris is parametrized while collecting frequencies of the peak of the S-parameters. This will get two peaks at different frequencies, calling f_h the peak at bigger frequency and f_l the one at the lowest.

Depending on how coupled it is the port to the resonators I can use S_{21} or S_{11} peaks, but I noted that it's better to use the first one because there some cases where peaks at S_{11} can overlap when they are very close, losing accuracy of our study.

When p increases, different peaks on the S_{21} move across the graph while one of them remains mostly still (Fig. 19).
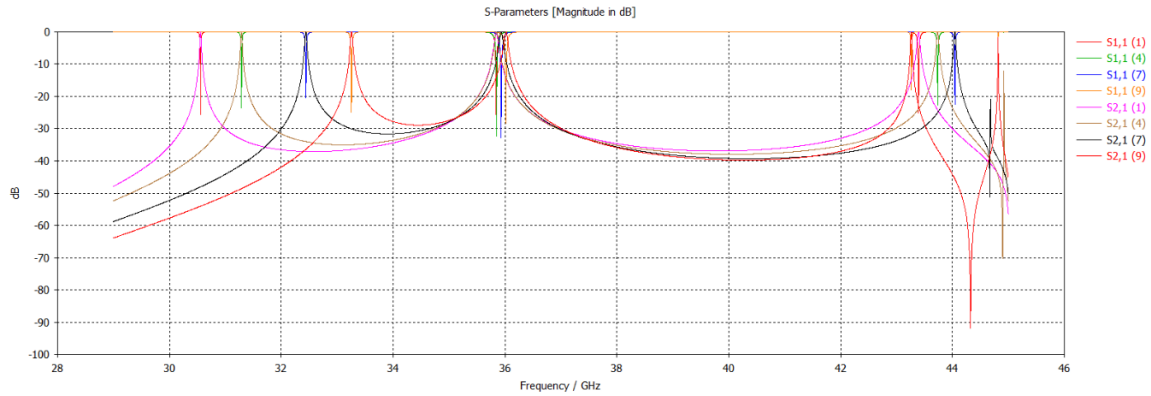

Figure 19: Evolution of S Parameters

Two of these peaks must be chosen, being resonant frequencies on the inter-resonator. They allow us to get the coupling coefficient (16).

$$K_{ij} = \frac{f_h{}^2 - f_l{}^2}{f_h{}^2 + f_l{}^2} \qquad (16)$$

This relation marks the interdependence of two cavities.

Inspired by papers where Python is used to optimize results [22] and realizing that CST online help has plenty of documentation about it, I decided to program a Python script that will solve the problem for this coefficient and the input coupling Q_{ext}, in order to save time and gain resolution.

3.2.1 Coupling factor K_{ij}

I wrote a script that autonomously changes parameters, simulates, gets the desired values and calculates the coefficient K_{ij} to later exports it to an Excel spreadsheet. In the end I found a bit more useful changing the script so it solely would gather and operate with results. (see Appendix 7.1)

As outlined before, depending on p, f_l and f_h would move along the graph, so what this program does is basically:

      -Execute certain macro to run a parametrized simulation.

      -Obtain the values from each simulation (parameter values, frequencies, amplitudes…)

      -Choose the frequency with a maximum amplitude in dB

      -Calculate the coupling coefficient

      -Save everything in a spreadsheet

      -Plot the graph relating iris length and coefficient.
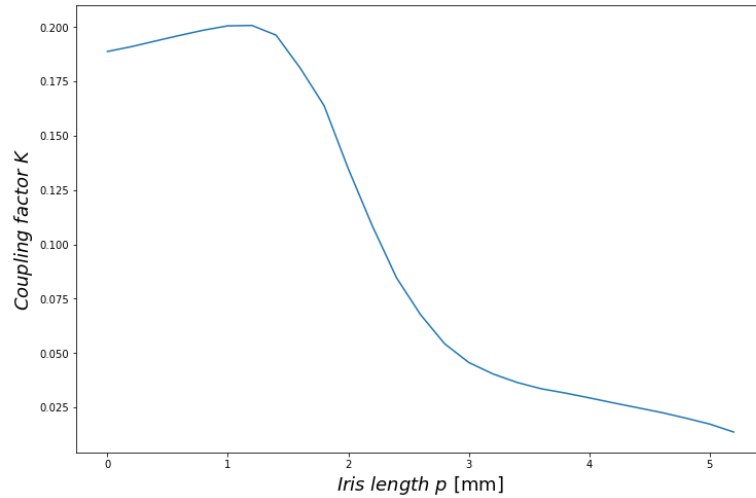
After a parametric sweep, the graph obtained (Fig. 20).


Figure 20: Final plot of Coupling coefficient

3.2.1.1 OBSERVATIONS

Even if this task seems minor, it brought several issues up:

(1) Choosing the best way to have ports weakly coupled:

I thought the best case would be when the lowest energy possible would be transmitted to the inter-resonator. I tried different ways to achieve this goal, one of them putting an iris between the port and first cavity, but it didn't work

I understand what it did was creating parasitic inductances that polluted the graph and shifted the resonant peaks to different values (Fig. 21).
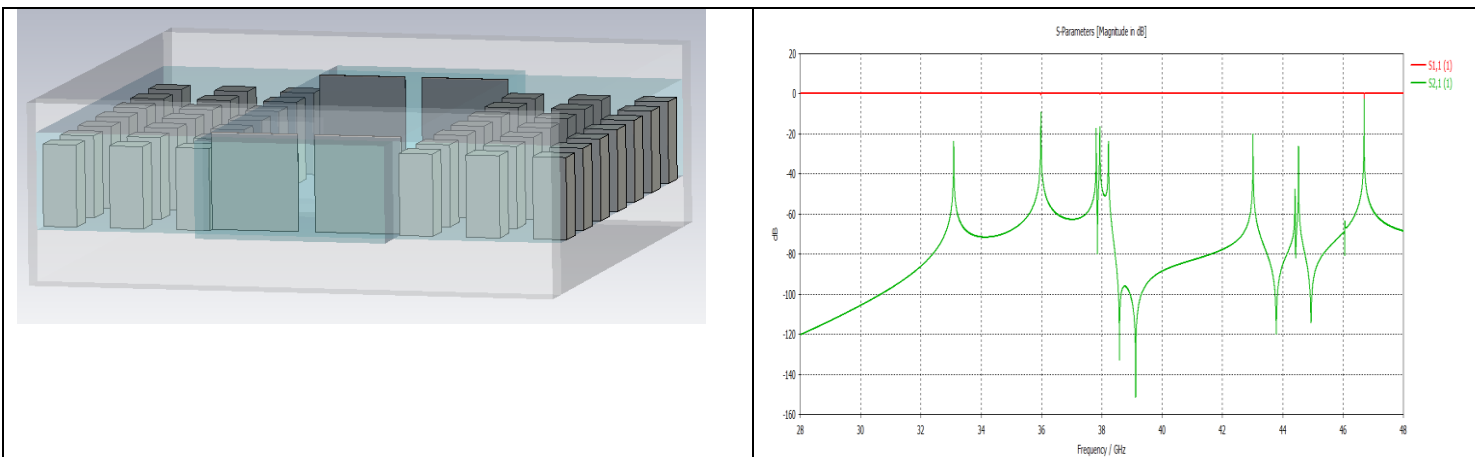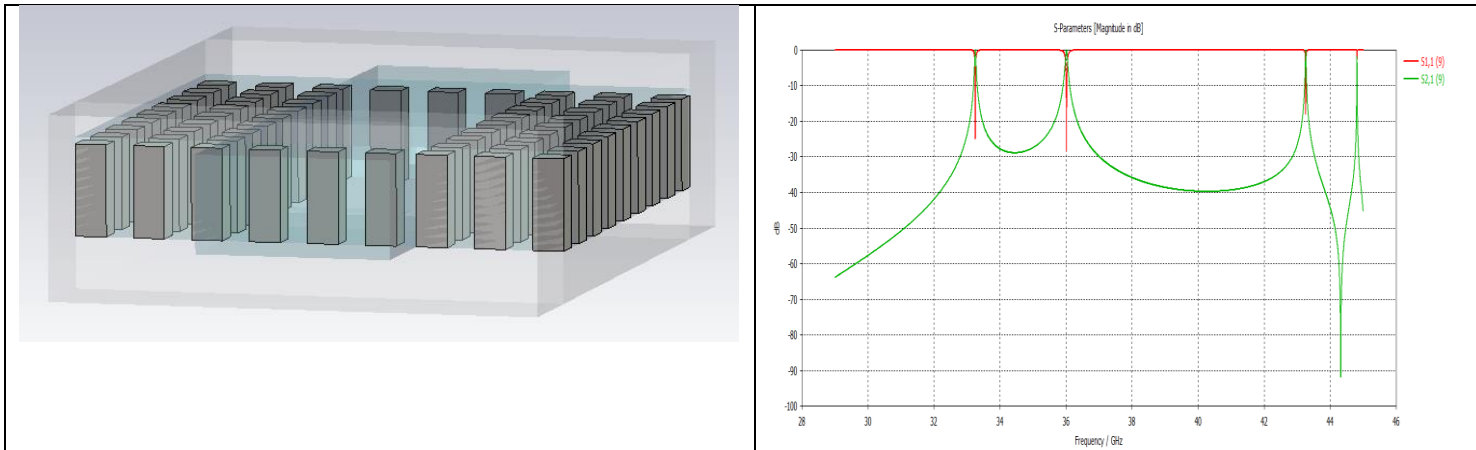
Figure 21: Comparison different ways of weak coupling.

Width of the input/output pins is important. I decided to make the thinnest but then some peaks appeared across the graph. I also parametrized their height trying to reduce the high frequency peaks, but that didn't improve whatsoever. I left them as the rest of the metal pins making a h = 0.445 mm gap.

(2) Choosing the correct peaks

Firstly, I picked the two tops at lowest frequency but results didn't end in a good filter.

I had to restart the process, then set different monitors up to observe the electric field at those frequencies. It became obvious I had chosen wrong maximums, seeing a mode resonating between the two cavities at the lowest frequency (Fig. 22).

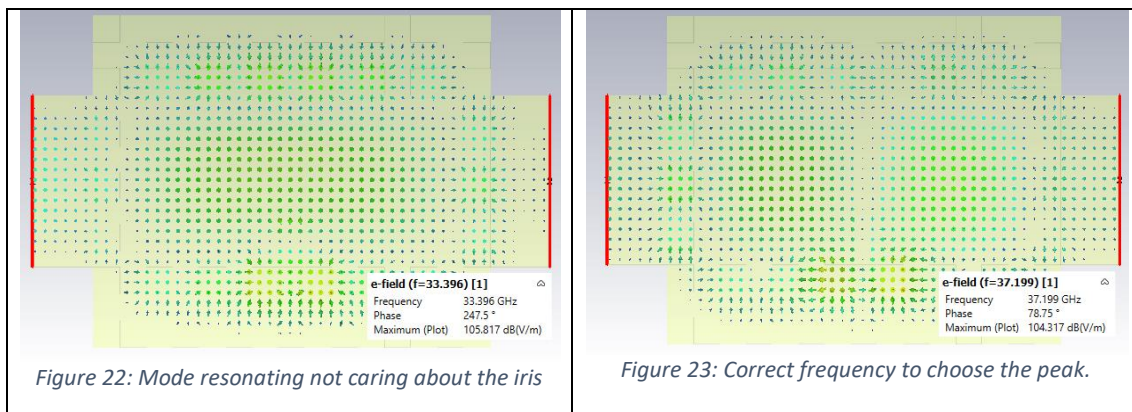After this process, results were consistent and accurate.

Figure 22: Mode resonating not caring about the iris

Figure 23: Correct frequency to choose the peak.

(3) Choosing the best gap

Although I knew that's mandatory to establish a fixed environment arranging parameters (gap, size of the metal pins or separation between them) and respect it to get the coherent solutions, I wanted to test how the coupling factor would be affected by the gap between pins

25

and the upper plate (*h*). The steep of the graph notably changed, what would result in very similar iris length to get distant value of coupling factor.

If so, any filter designer would like to get a gentle curve at values of coupling factor near their needs. If not, maybe it will turn out that very similar irises will be required for disparate K_{ij}.

In Fig. 24 is possible to appreciate this difference. Also, there are certain coupling factors that are not available depending on the gap size, a designer should consider this trade off.
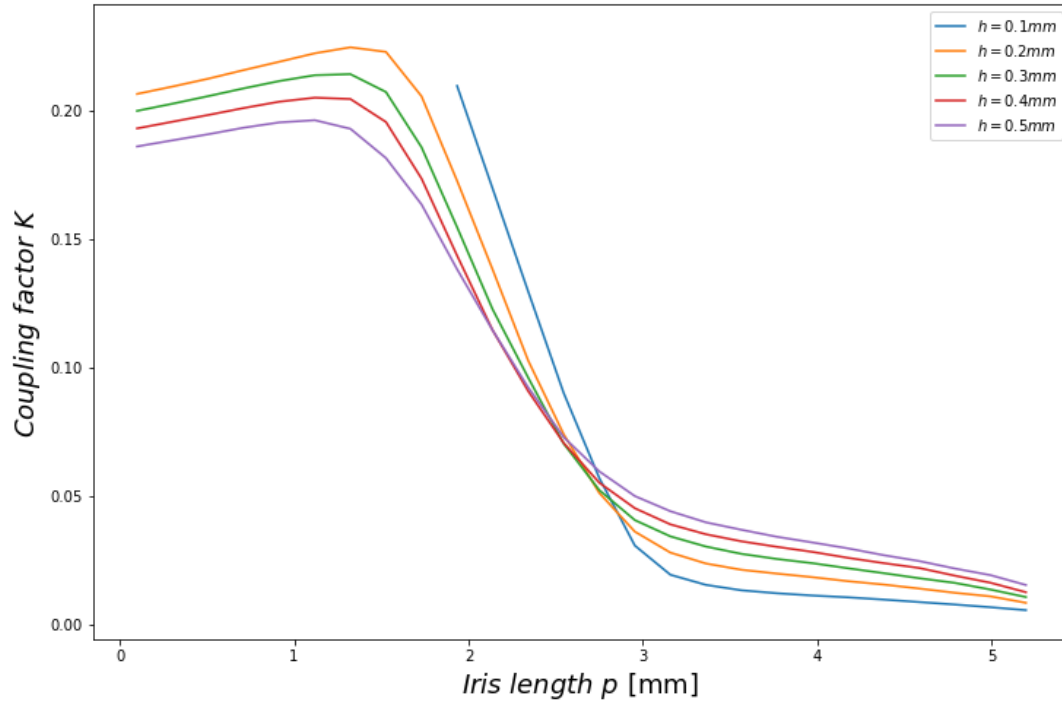

Figure 24: Variation of coupling factor VS. h

3.2.2   Input coupling Q_{ext}

In this case, I designed a second mini resonator (Fig. 25) and set an iris in between two same-length cavities, 5.67 mm as before.
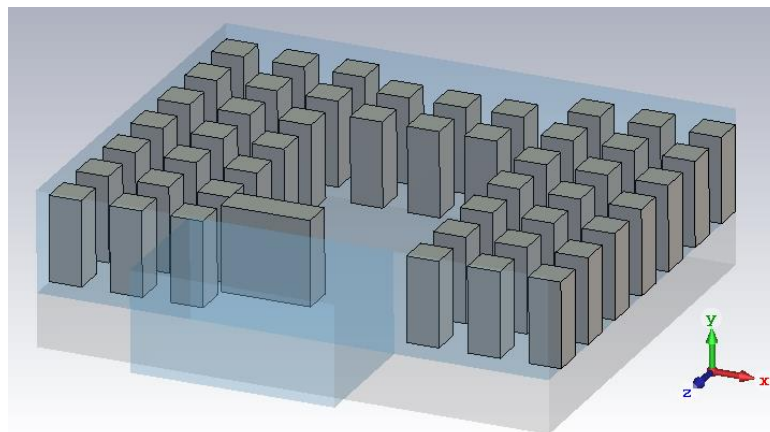

Figure 25: 3D view

26

There are two methods to obtain the input coupling. One of them rests in the ±90° phase shift($\Delta f_{\pm90}$) respect resonant frequency on the S_{11}. Then (17) can calculate the coefficient.

$$Q_{ext} = \frac{f_0}{\Delta f_{\pm90°}}$$ (17)

However, I knew that the iris loading could affect to the f_0 of the cavity.

I set this feature aside because I planned to optimize values after the filter would be made (to get the best and centred response), but now couldn't decide what exact frequency I should use at this point.

The second approach obliterate this problem: The group delay method. Thanks to CST I could review the group delay τ_g results and choose the frequency with the biggest value of delay group.

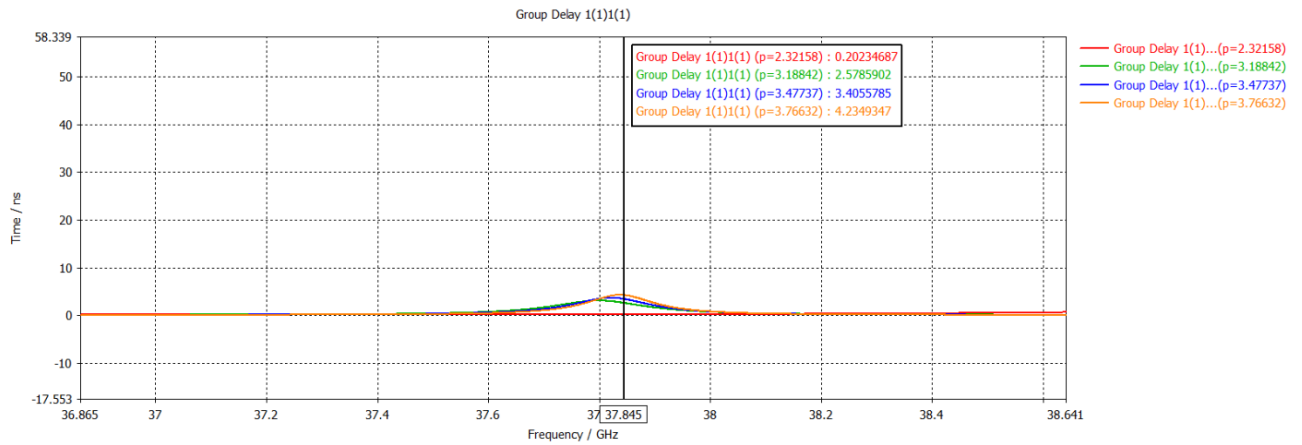When p is increased, τ_g has a maximum moving across the graph (Fig. 26).

Figure 26: Evolution of τ_g

Then I reviewed literature, specially [23] and I decided to use (16)

$$\tau_{S_{11}}(f_0) = \frac{4\,Q_e}{2\pi f_0}$$ (18)

Hence,

$$Q_{ext} = 2\pi f_0 \frac{\tau_{S_{11}}(f_0)}{4}$$ (19)

The program had (19) in account and made the math (see Appendix 7.2)

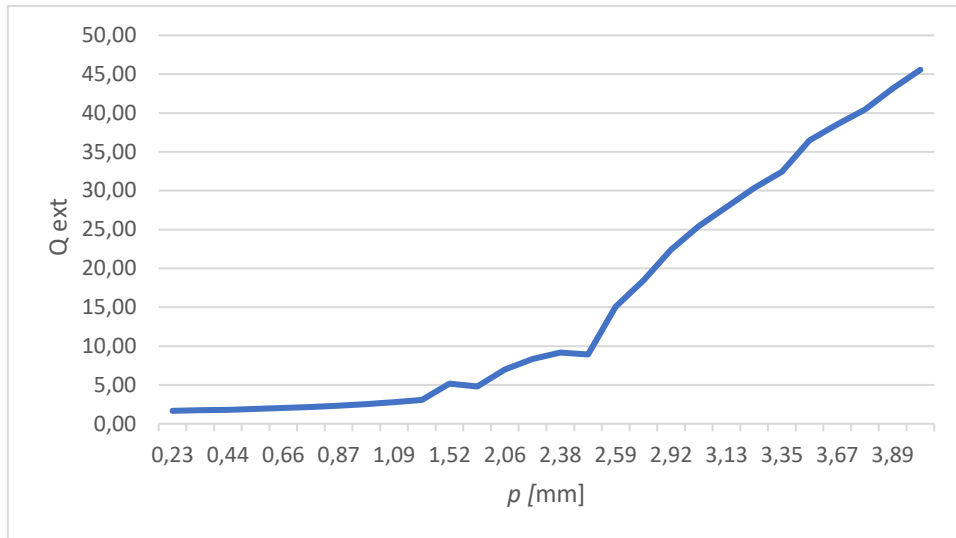In this case, the evolution of Q_{ext} is shown on Fig. 27

Figure 27: Q_{ext} VS. p

3.3   DESIGN OF COUPLED RESONATORS WAVEGUIDE FILTER

Thanks to previous study, it was possible to relate the wanted behaviour to the specific dimensions:

Table IV: Measures of desired filter	
Coupling coefficient K_{ij}	**Iris length**
Q_{ext} = 24,39	l_1 = 2.95 mm
K_{12} = K_{45} = 0.0347793	l_{12} = 3.5 mm
K_{23} = K_{34} = 0.025551	l_{23} = 4.3 mm

The length of resonant cavities was 5.67 mm

The response didn't fulfil a filter minimum requirement so we optimized all the values, effecting on dimensions (Fig. 28), so a 5th order Chebyshev filter with the final stated characteristics would change its S11 as is depicted in Fig. 29.

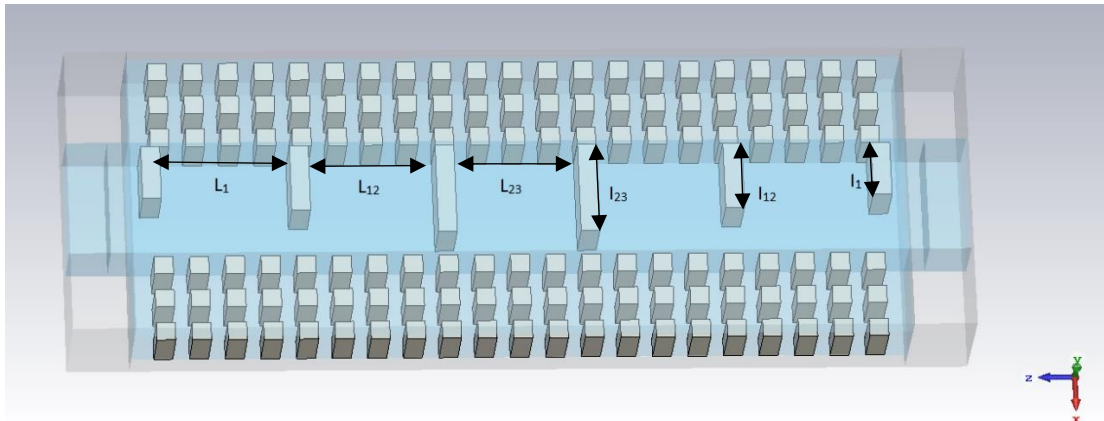| Table V: Measures after optimization		
Resonator	**Iris length**	**Cavity length**
Cavity 1	l_1 = 2.68 mm	L_1 = 6.21 mm
Cavity 2	l_{12} = 3.01 mm	L_{12} = 5.97 mm
Cavity 3	l_{23}= 3.53 mm	L_{23} = 5.90 mm

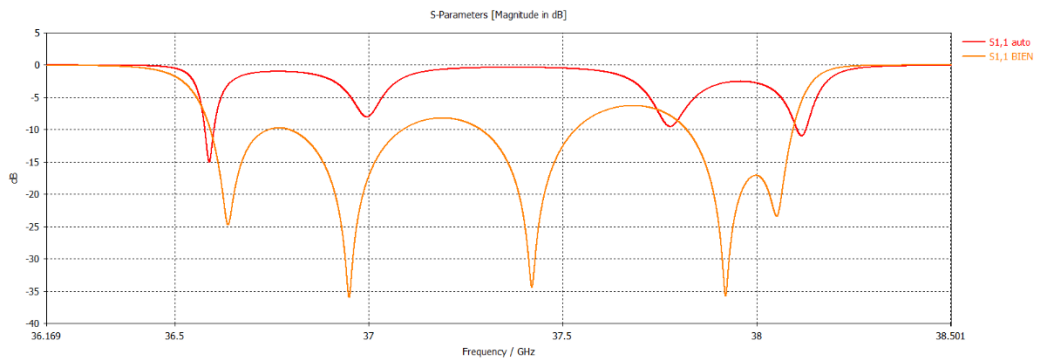*Figure 28: 3D view of filter with variables (see Table 5)*

Figure 29: S11 Before (auto) and after (BIEN) optimization

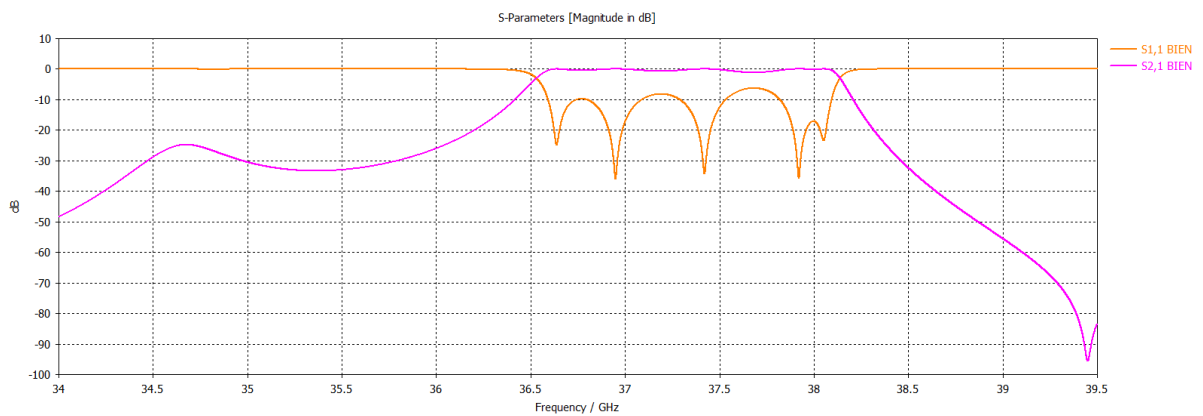In Fig. 30 there is the magnitude response and after the optimization.

Figure 30: S-Parametres after optimization

4.   STUDY OF OVERMODED CAVITIES WAVEGUIDE FILTERS

As it is stated in Chapter 1, physical dimensions fix the frequency in waveguides, and they normally only propagate the fundamental mode.

Although, new type of filters where better insertion losses and selectivity can be achieved by creating oversized cavities along with standard ones.

In this manner, higher order resonant modes are present. There is in Fig. 31 the representation of electric field in two modes TE_{201} TE_{301}, if we think the order of indexes are TE $_{y\,z\,x}$.

It's trivial to see the half-wavelength phase reversal in the higher mode, so it could be used to create a cross coupling for the fundamental previous mode if both modes would resonate within same cavity at same frequency.
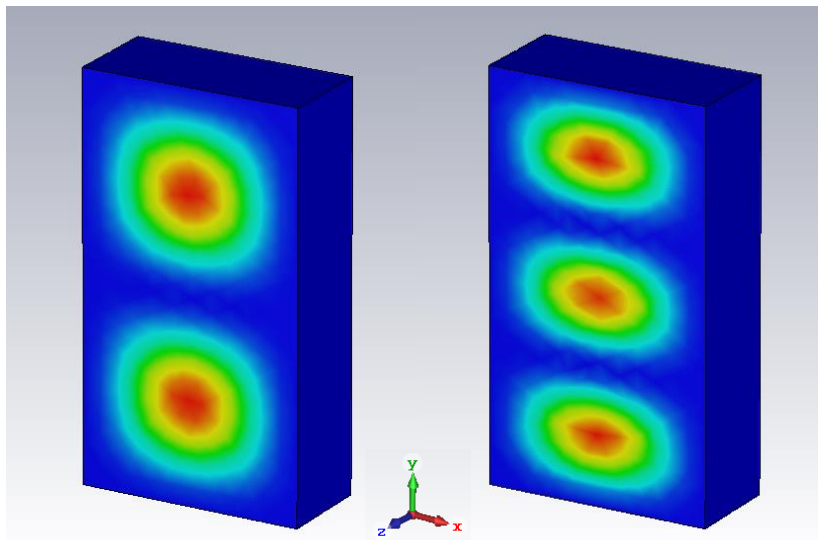

Figure 31: Physical electric density of TE_{102} TE_{103}

If we place a central post in these oversized cavities it would act as a dielectric, lowering the high order mode's resonant frequency.

If two cavities are constructed with a bigger cavity between them, we could propagate a lower resonant mode (TE_{101}) within first and third cavity bypassing the overmoded cavity.

Thus, could be possible to profit of the cross-coupling while exiting with same mode as in the input port. There are examples where there is a Chebyshev filter with central frequency $f_0 = 10$ GHz and bandwidth *BW = 400* MHz within WR90 waveguide, which operates between 8-12 GHz [10].

In this example, this kind of filter is proposed in GGW.

4.1   ANALYSIS

A cavity with WR90 dimensions (*a = 22.86 mm* wide and *b = 10.16 mm* high) is built with *d = 41mm* long (Fig. 32).
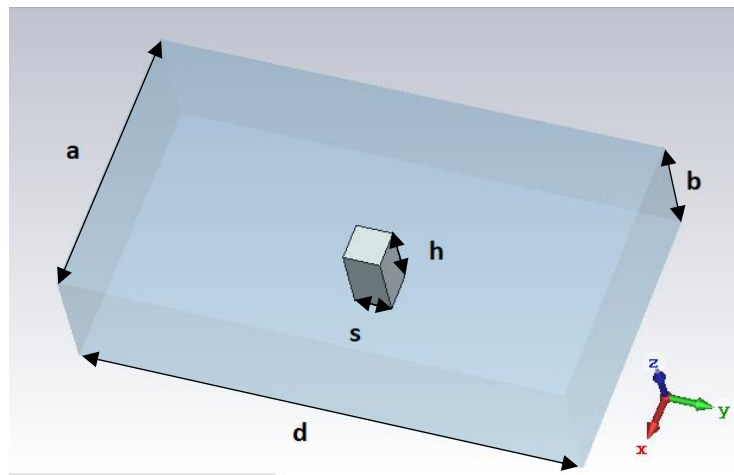

Figure 32: 3D view of the resonator

$$f_{lnm} = \frac{c}{2\pi\sqrt{\mu r\; \epsilon r}}\sqrt{\left(\frac{l\,\pi}{d}\right)^2 + \left(\frac{n\,\pi}{b}\right)^2 + \left(\frac{m\,\pi}{a}\right)^2} \qquad (20)$$

If we apply (20) we can calculate the modes which resonate at that cavity.
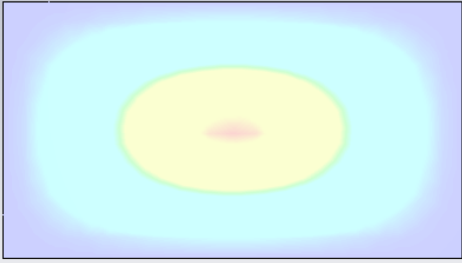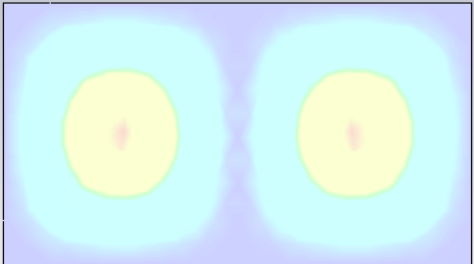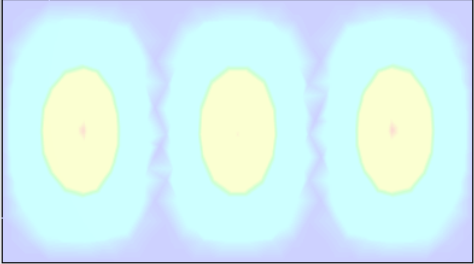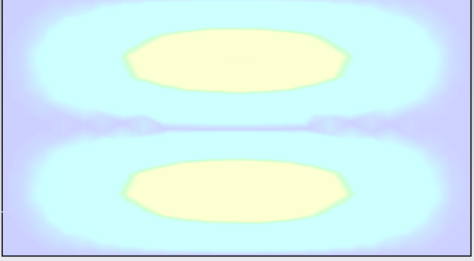
$$TE_{101} = 7.51269 \text{ GHz}$$

$$TE_{201} = 9.8283 \text{ GHz}$$

$$TE_{301} = 12.7875 \text{ GHz}$$

Eigensolver simulation verifies it and also plots the physical distribution of field, in this case the density of electrical energy.

The first modes which appear are the different expressions of the fundamental TE_{10} and TE_{20}, each of them resonates at different frequency (Table 6).

Table VI: Eigensolver for regular WR90		
MODE	**FREQ**	**ELECTRICAL DENSITY**
TE_{101}	7.50 GHz	
TE_{201}	9.82 GHz	
TE_{301}	12.77 GHz	
TE_{102}	13.61 GHz	

However, when a square post (*s = 3mm*) is placed in the centre of the cavity the resonant frequency of the modes who are physically disturbed by it would change the frequency of resonance. (Fig. 32)

In this particular case, the influence of central post's height *h* on the central lobe mode of TE_{301} and TE_{101} gradually decreases the resonance frequency.

A parametric sweep (*h* → [0-9] mm) is performed to evaluate the variation of these modes.

In Fig. 33 it's plotted the deviation of the cut-off frequency, where TE_{301} resonant frequency decreases until it's almost the same as TE_{201}. The other two modes remain unaffected because the central post is placed where occurs a minimum of electric field for them.

Thus, it's achievable to get two different order modes resonating at the same frequency.
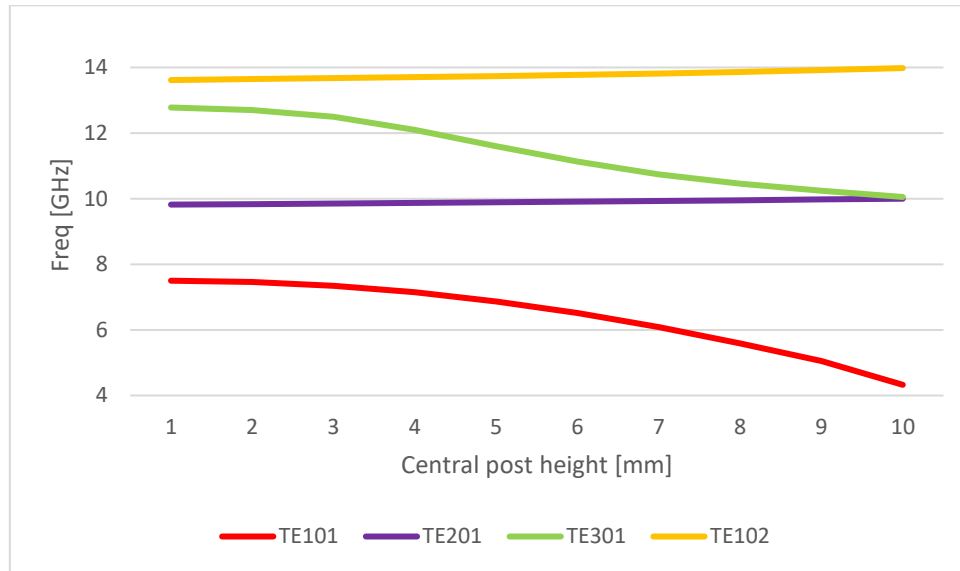
Figure 33: Modes vs. height of central post in regular WR90

Afterwards, a GGW waveguide is built. Two rows of square pins (*wPin = 2.1* mm side, *hPin = 9.38* mm high) are positioned with *distPin = 1.785 mm* distance between them (Fig. 34)

Pins height *hPin* matches λ/4 of 8 GHz, they are chosen to avoid energy propagation from 8 GHz. Distance between them and side are chosen to bring the best bandgap following same guides as in Chapter 2.2.1, selected to improve bandgap until 14 GHz, the upper boundary before multimode.
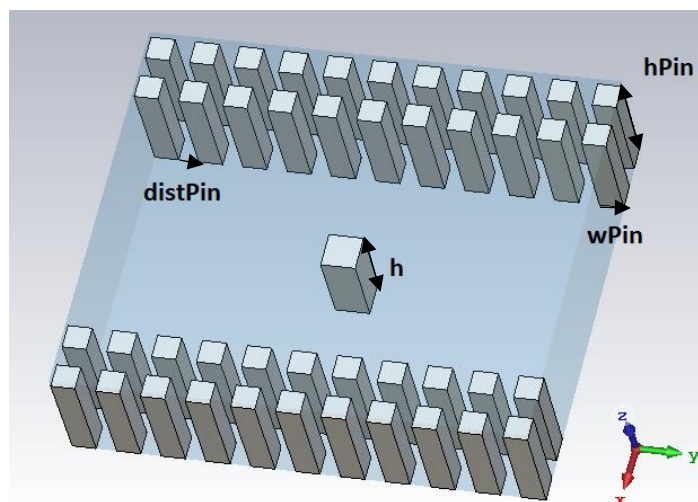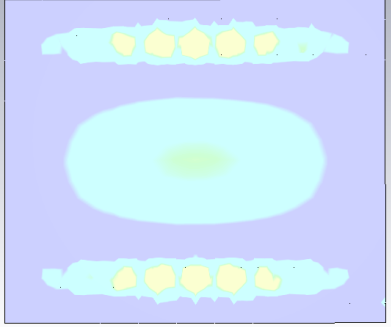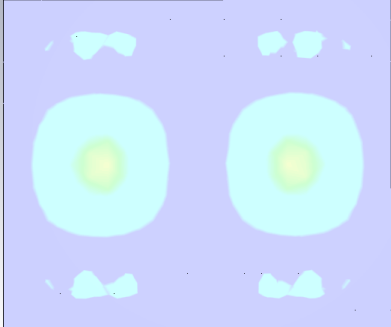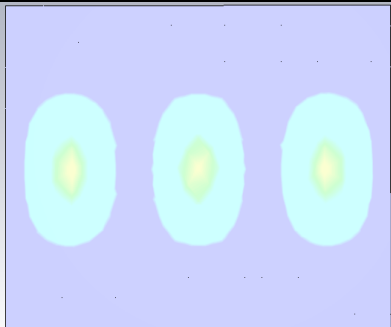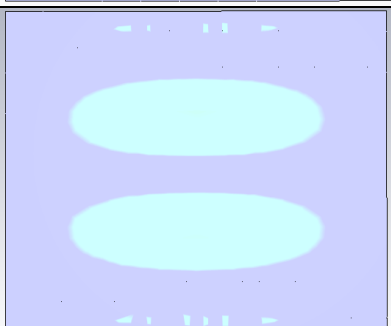
Figure 34: 3D view of WR90 resonator

Eigenvalues results of the groove resonator are analysed (see Table 7), looking for the expression of aforementioned modes. The only noticeable change is the frequency shift of the first mode of interest, the rest of aspects remain similar.

Table VII: Eigensolver for GGW WR90		
MODE	**FREQ**	**ELECTRICAL DENSITY**
TE_{101}	7.85 GHz	
TE_{201}	9.90 GHz	
TE_{301}	12.745 GHz	
TE_{102}	13.35 GHz	

Again, a central post is placed in the middle of the waveguide with exact same side size ($s = 3$ mm). The evolution of results after parametric sweep of h (from 0 to 9 mm) can be seen in Fig. 35.

Same changes between modes TE_{301} and TE_{201} happens when reaching high values in the central post, having similar resonance frequencies while being different modes.

After this analysis, we can conclude the same design will work with GGW technology.
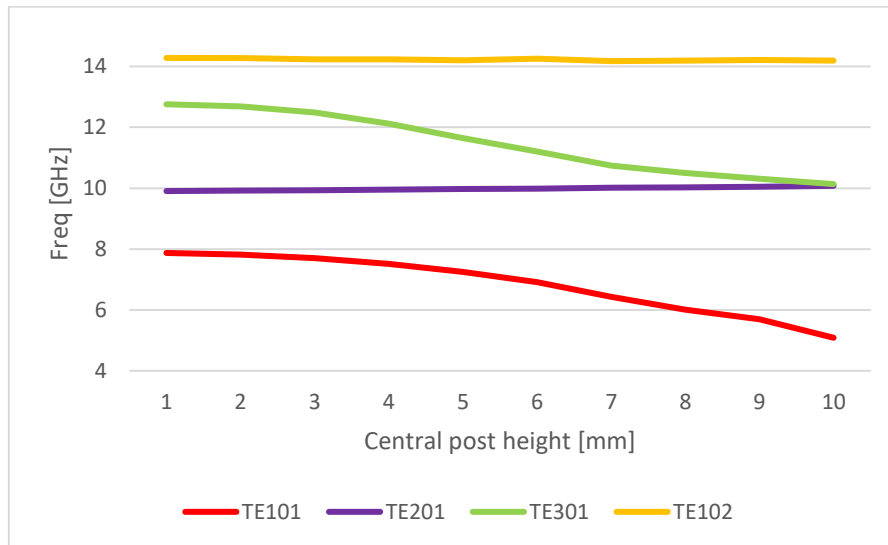
Figure 35: Shift of resonances in GGW WR90

As a final point, we asserted groove gap technology would help to avoid physical imperfections noticeable from certain range of frequencies. There is no need to use GGW at frequencies around 10 GHz.

Consequently, exact same experiment is delivered at a groove WR22 expecting same results. Frequency of interest is the resonance of mode TE_{201}, then (18) is applied to make it resonate at 35,3 GHz, resulting in length *d = 14.22* mm.

Cavity formed by *a = 5.6896* mm, *b = 2.8448* mm and similar design of pins as in Chapter 1 (*distPin* = 0.76 mm, *wPin* = 0.9 mm, *hPin* = 2.27 mm) with a central post with side *s = 1.27* mm performs a parametric sweep.

Unsurprisingly, results are positive, confirming our hypothesis (Fig. 36)
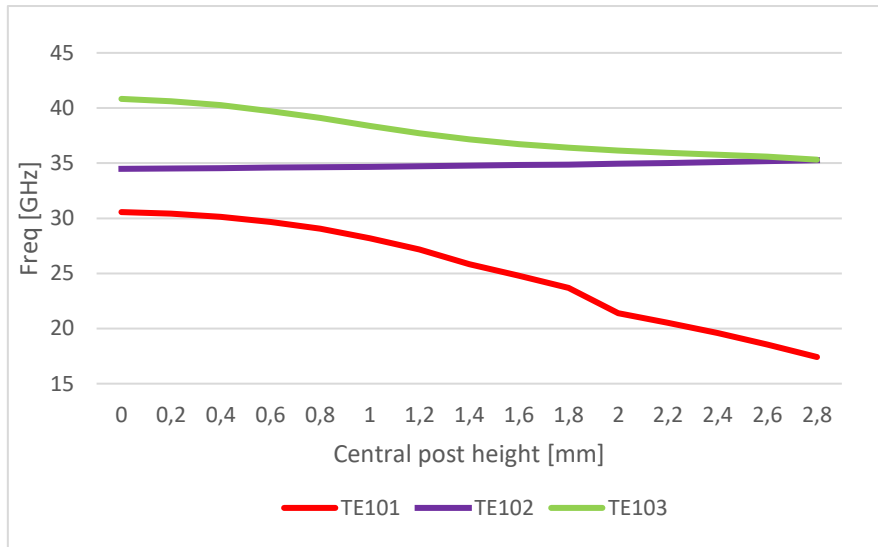
Figure 36: Modes vs central post height in GGW WR22

4.2 FOUR-POLE FILTER

A solution to design narrow band filters is introducing TZ by designing asymmetrical structures as well as having overmoded cavities. In [10] it is explained how four different frequency response can be obtained with the same kind of filter, depending on choosing particular parameters from its structure, e.g. offset *o* (Fig. 38).

For instance, a four-pole filter was designed setting two cavities with a large *o,* creating great uncoupling between resonant and non-resonant modes between cavities. This would create a very selective response without TZ next to passband (Fig. 37)
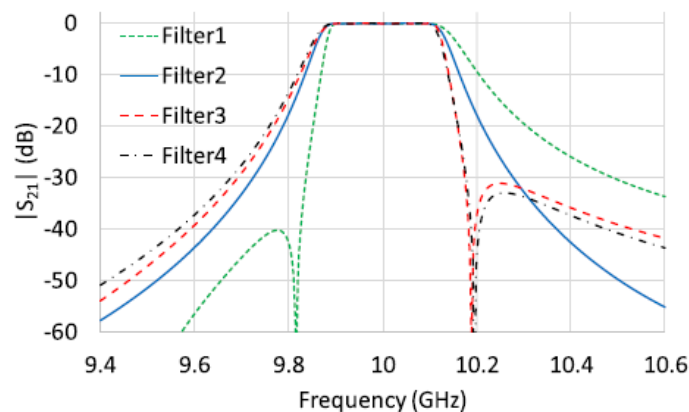
Figure 37: Four frequency responses that can be obtained with filter proposed in [10].

In this section, I use the concepts already proven to reproduce an example of these filters now with groove technology: a device formed by three cavities, the one in the middle bigger (overmoded), creating four-pole filter working around 10 GHz.

The first step is designing with magnitudes shown on the mentioned paper (see Table 8), as well as the already known for GGW WR90 (Fig. 17)

Table VII: Significant measures of 4-pole filter	
Bound	Value [mm]
w1	10.80
w2	7.10
t	16.84
s	40.30
o	8.60
l1	9.00
h	3
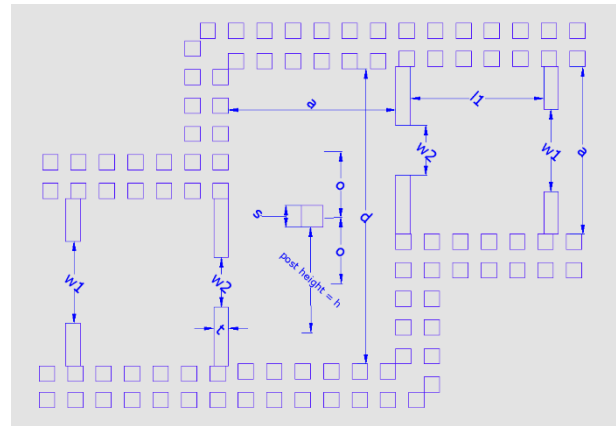
Figure 38: Top view of filter with measurements
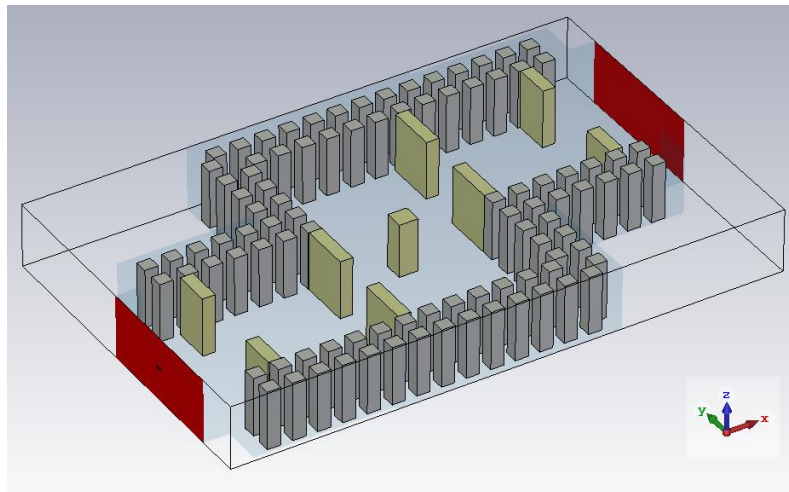
Figure 39: 3D view. File with extension .cst is available for clarification.

The response of the filter (Fig. 40) has a bandpass at 10 GHz and a TZ on the right of it.

This kind of filters normally bring a TZ, depending on the relative position of the cavities (which are established by offset *o*) but also it's possible to bring a shape response with no TZ near the bandpass, as mentioned before.

In any case, this proved the viability of applying groove gap technology in this type of structure, getting valid responses, despite the changes that surely groove can cause on the response. A specific study about position and offset likewise groove gap is required as a further line of investigation.
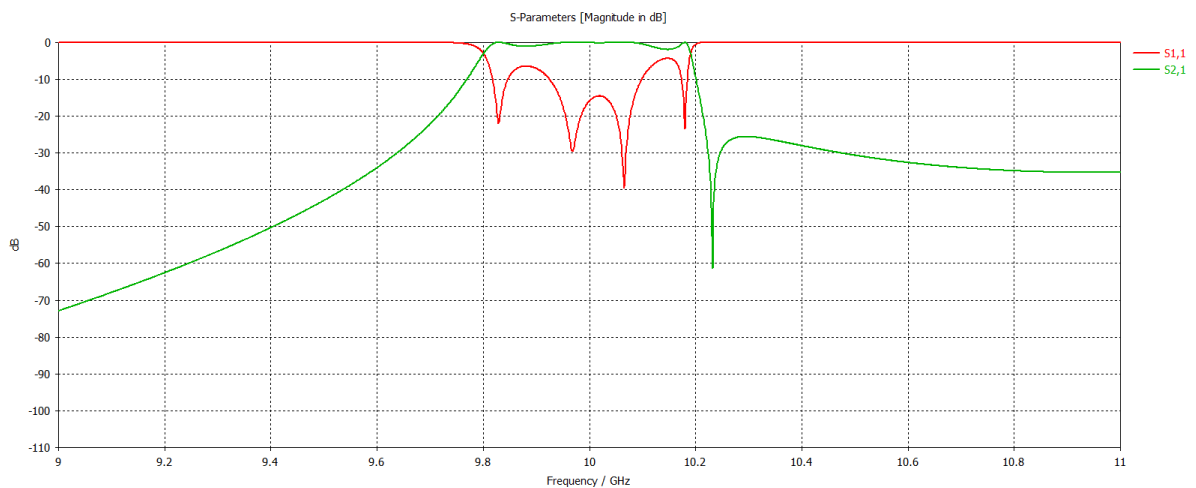
Figure 40: Response of the four-pole filter with GGW

It could work at higher frequencies like standard WR22 as we have verified the basis of performance in the previous part but it would necessary some more alignments. Unlike WR22, this waveguide's height and width relation is not exactly double, so even taking this in account it would not be as easy as just scaling values in CST Studio.

Even so, it is demonstrated the feasibility of GGW along with complex filters like this one.

5.   CONCLUSIONS

This end-of-degree work helped me to have a different view of how waveguides are constructed. During the time I studied Signal Processing I learned the implications of lumped elements in the magnitude and phase response, but they were more concepts to work in a piece of paper.

However, after these four months I reviewed that theory about before I acknowledged brand new concepts way more real and practical.

At this day, I distinguish that if I only change height of the pins intended for make weak coupling will only change the amount of energy but not resonant frequencies.

I have a proper knowing about how to model with CST and not to forget to check parameters who will affect to the response if they are not correct. Type of mesh, boundaries, symmetries…

Yet mathematical expression of electromagnetic fields was not scrutinized (an example of that is the lack of them in this work) I believe I have a better spatial and conceptual vision of modes.

On the other hand, I wish I could have time for deepening into the ideas regarding the last chapter. I will have to wait to know more about multiple coupling and the tools to standardise design of this form of filters.

I would like to have presented better S-parameters response but I had issues regarding the computer's RAM memory when I tried to do in general mode and adaptive mesh cell division.

6.   FUTURE LINE

Study analysing and testing the frequential performance with this novel fabrication technique (SLM) and material (Scalmalloy®) to characterize it.

Also, as future line I would like to advance in a procedure to build waveguide filters with cavities where are resonant and non-resonant modes are present. This method would analyse multiple coupling between hollows and the procedure to insert transmission zeros (TZs) next to the bandpass, helping the overall response.

7. APPENDIX

7.1 Coupling_factor.py

```python
### COUPLING FACTOR.PY
# Joseph Zandueta
# Este programa simula y cambia el parámetro elegido, en este caso p.

# Importacion de librerias necesarias
import os
import sys
sys.path.append(r"C:\Program Files (x86)\CST Studio Suite
2020\AMD64\python_cst_libraries")
import cst.interface
from cst.interface import Project
import cst.results
import matplotlib.pyplot as plt
%matplotlib inline
import numpy as np
import cst
import pandas as pd
import numpy as np

#PRIMERA PARTE

ruta = str(r'[ruta a la carpeta de los proyectos .cst]')
file= str(r'[nombre_archivo].cst')

#Se inicia el programa CST y se accede al proyecto.
mycst = cst.interface.DesignEnvironment()
mycst1=cst.interface.DesignEnvironment.open_project(mycst, ruta+file);

#Estos serán los valores que tome el parámetro, en este caso p
valP= pd.Series(np.arange(0,5.68,0.05));

columns=['Frecuencias', 'Factor Acoplamiento (K)', 'Longitud p' ,'Amplitudes',
'Angulo', '%BW'];
resultados=pd.DataFrame(columns=columns);

n=0;
f0=37.2;

#Codigo VBA que ejecuta cada simulacion
for num in valP:
    par_change = 'Sub Main () \nStoreParameter("p",
'+str(num)+')\nRebuildOnParametricChange (bfullRebuild, bShowErrorMsgBox)\nEnd Sub'
    mycst1.schematic.execute_vba_code(par_change, timeout=None) #execute VBA script
    cst.interface.DesignEnvironment.in_quiet_mode = False

    mycst1.modeler.run_solver()    #run simulation
    project = cst.results.ProjectFile(ruta+file, allow_interactive=True)
#allow_interactive permite que se vuelva a ejecutar sin necesidad de cerrar CST

    #SEGUNDA PARTE

    S21 = project.get_3d().get_result_item(r"1D Results\S-Parameters\S2,1")
    xD=np.array(S21.get_xdata());

    y=20*np.log10(np.array(S21.get_ydata()));
    yReal,yImag= np.real(y), np.degrees(np.angle(y));

    df= pd.DataFrame({'freq':xD, 'abs':yReal, 'phase':yImag})
```

```python
    abss=[]
    freqs=[];
    angles=[];

    #Selecciono los maximos y evito los picos de bajas frecuencias que no aportan
    #Voy guardando los datos de esos maximos
    for x in df.index[1:-1]:
        if(df.loc[x,'abs']>df.loc[x+1,'abs'] and df.loc[x-1,'abs']<df.loc[x,'abs']
and df.loc[x,'abs']>-40 and df.loc[x,'freq']>35.39):
            freqs.append(df.loc[x, 'freq']);
            abss.append(df.loc[x, 'abs']);
            angles.append(df.loc[x, 'phase'])

    abss=np.array(abss)
    freqs=np.array(freqs) #.astype(np.float)
    angles=np.array(angles)

    #Ordeno en funcion de la cercania a f0 para saber cuales son los dos picos
    df2=pd.DataFrame({'freq2':freqs,'abs2':abss,'phase2':angles});
    df2=df2.sort_values(by=['freq2'], key= lambda x: np.absolute(f0-
x),ignore_index=True) #ignore_index resetea los indices despues de ordenar

    resultados.loc[n,'Amplitudes']=np.array(df2['abs2'][:2])
    resultados.loc[n,'Frecuencias']=np.array(df2['freq2'][:2])
    resultados.loc[n,'Angulo']=np.array(df2['phase2'][:2])

    resultados.loc[n,'Longitud p']= num
    aux=np.power(resultados.loc[n,'Frecuencias'],2)

    try:
        kF= (aux.max()-aux.min())/(aux.max()+aux.min()); #Salvamos el error cuando
no hay ningún valor bueno
        resultados.loc[n,'%BW']= np.absolute(freqs[0]-freqs[1])/f0 * 100

    except Exception as e:
            kF=np.nan;
    resultados.loc[n,'Factor Acoplamiento (K)']= kF

    n=n+1;

cst.interface.DesignEnvironment.close(mycst) #Permite cerrar la instancia del
simulador

# TERCERA PARTE
resultados.to_excel('DATOS 21 FACTOR ACOPLO '+file[1:]+'.xlsx');

var_file=r'datos S21 FACTOR ACOPLO'+file[1:]+'.xlsx'
resultados = pd.read_excel (var_file);
y= resultados['Factor Acoplamiento (K)']
x= resultados['Longitud p']
fig, ax = plt.subplots(figsize=(12, 8))
ax.set_xlabel(r'$Iris$ $length$ $ p$ [mm] ', fontsize=18)
ax.set_ylabel(r'$Coupling$ $factor$ $K$', fontsize=18)
ax.plot(x,y);
```

```python
### VERSION 2
# En esta versión se recogen los datos de la simulacion
# Estan marcadas las ordenes diferentes
###

project = cst.results.ProjectFile(ruta+file, allow_interactive=True) #Permite que
se vuelva a ejecutar sin que se cierre CST
#Recoge la lista de simulaciones
lista_ids= project.get_3d().get_run_ids(r"1D Results\S-Parameters\S1,1");
```

```python
n=0;

columns=['Frecuencias', 'Factor Acoplamiento (K)', 'Longitud p' ,'Amplitudes',
'Angulo', '%BW'];
resultados=pd.DataFrame(columns=columns);
freq_central=35.39;

for num in lista_ids[x:y]: #Puede que no nos interesen todas las simulaciones
    S21 = project.get_3d().get_result_item(r"1D Results\S-Parameters\S2,1", num)
    xD=np.array(S21.get_xdata());

    y=20*np.log10(np.array(S21.get_ydata()));
    yReal,yImag= np.real(y), np.degrees(np.angle(y));

    df= pd.DataFrame({'freq':xD, 'abs':yReal, 'phase':yImag})
    abss=[]
    freqs=[];
    angles=[];

    for x in df.index[1:-1]:
        if(df.loc[x,'abs']>df.loc[x+1,'abs'] and df.loc[x-1,'abs']<df.loc[x,'abs']
and df.loc[x,'freq']>freq_central and df.loc[x,'abs']>-40):
            freqs.append(df.loc[int(x), 'freq']);
            abss.append(df.loc[int(x), 'abs']);
            angles.append(df.loc[int(x), 'phase'])

    abss=np.array(abss)
    freqs=np.array(freqs) #.astype(np.float)
    angles=np.array(angles)

    df2=pd.DataFrame({'freq2':freqs,'abs2':abss,'phase2':angles});
    df2=df2.sort_values(by=['freq2'], key= lambda x: np.absolute(freq_central-
x),ignore_index=True)

    resultados.loc[n,'Amplitudes']=np.array(df2['abs2'][:2])
    resultados.loc[n,'Frecuencias']=np.array(df2['freq2'][:2]) #.astype(np.float)
    resultados.loc[n,'Angulo']=np.array(df2['phase2'][:2])


    resultados.loc[n,'Longitud p']=
project.get_3d().get_parameter_combination(num).get('p');
    aux=np.power(resultados.loc[n,'Frecuencias'],2)
    try:
        kF= (aux.max()-aux.min())/(aux.max()+aux.min()); #Salvamos el error cuando
no hay ningún valor
        resultados.loc[n,'%BW']= np.absolute(freqs[0]-freqs[1])/freq_central * 100
    except Exception as e:
        kF=np.nan;
    resultados.loc[n,'Factor Acoplamiento (K)']= kF


    n=n+1;
resultados.sort_values(by=['Longitud p'], inplace=True)
resultados.to_excel('Rescate S21 FACTOR ACOPLO'+file[1:]+'.xlsx');
var_file=r'Rescate S21 FACTOR ACOPLO'+file[1:]+'.xlsx'
resultados = pd.read_excel (var_file);
y= resultados['Factor Acoplamiento (K)']
x= resultados['Longitud p']
fig, ax = plt.subplots(figsize=(12, 8))
ax.set_xlabel(r'$Iris$ $length$ $ p$ [mm] ', fontsize=18)
ax.set_ylabel(r'$Coupling$ $factor$ $K$', fontsize=18)
ax.plot(x,y);
```

7.2. Input_Coupling.py

```python
### INPUT COUPLING.PY
# Joseph Zandueta
# DELAY DE GRUPO y utilizando los resultados de las simulaciones

project = cst.results.ProjectFile(ruta+file, allow_interactive=True) #Permite que
se vuelva a ejecutar sin que se cierre CST
lista_ids= project.get_3d().get_run_ids(r"1D Results\S-Parameters\S1,1");

n=0;

columns=['Q ext', 'Longitud p', 't_max', 'w0'];
resultados=pd.DataFrame(columns=columns);

for num in lista_ids[2:]:
    auxtabla=project.get_3d().get_result_item(r"Tables\1D Results\Group Delay
1(1)1(1)",num);
    xtabla=np.array(auxtabla.get_xdata());
    ytabla=np.array(auxtabla.get_ydata());
    yReal= np.real(ytabla)
    dftabla= pd.DataFrame({'freq':xtabla, 'abs':yReal})
    freq_central= dftabla.loc[dftabla['abs']==dftabla['abs'].max()].freq.values
    #Cogemos el maximo de retardo de grupo
    t_max=dftabla['abs'].max();

    resultados.loc[n,'Longitud
p']=project.get_3d().get_parameter_combination(num).get('p');
    qext=(t_max/4)*freq_central # falta 2*np.pi
    resultados.loc[n,'Q ext']=qext;

    resultados.loc[n, 'w0']=freq_central;
    resultados.loc[n,'t_max']=t_max;
    n+=1
resultados.sort_values(by=['Longitud p'], inplace=True)
resultados.to_excel('RETARDO GRUPO Q_ext_datos '+file[1:]+'.xlsx');

var_file=r'RETARDO GRUPO Q_ext_datos '+file[1:]+'.xlsx'
resultados = pd.read_excel (var_file);

fig, ax = plt.subplots(figsize=(12, 8))
y= resultados['Q ext']
x= resultados['Longitud p']
ax.plot(x,y);
ax.set_title('Q ext');
```

8. BIBLIOGRAPHY

[1]   A. Díaz Morcillo, J. Fayos Fernández, and J. Monzó Cabrera, *Microondas: líneas de transmisión, guías de onda y cavidades resonantes*. 2016. Accessed: Feb. 04, 2021. [Online]. Available: https://lectura.unebook.es/viewer/9788416325061

[2]   K. S. Packard, 'The Origin of Waveguides: A Case of Multiple Rediscovery', *IEEE Trans. Microw. Theory Tech.*, vol. 32, no. 9, pp. 961–969, Sep. 1984, doi: 10.1109/TMTT.1984.1132809.

[3]   P. Kildal, E. Alfonso, A. Valero-Nogueira, and E. Rajo-Iglesias, 'Local Metamaterial-Based Waveguides in Gaps Between Parallel Metal Plates', *IEEE Antennas Wirel. Propag. Lett.*, vol. 8, pp. 84–87, 2009, doi: 10.1109/LAWP.2008.2011147.

[4]   A. U. Zaman, P.-S. Kildal, and A. A. Kishk, 'Narrow-Band Microwave Filter Using High-Q Groove Gap Waveguide Resonators With Manufacturing Flexibility and No Sidewalls', *IEEE Trans. Compon. Packag. Manuf. Technol.*, vol. 2, no. 11, pp. 1882–1889, Nov. 2012, doi: 10.1109/TCPMT.2012.2202905.

[5]   T. M. Mower and M. J. Long, 'Mechanical behavior of additive manufactured, powder-bed laser-fused materials', *Mater. Sci. Eng. A*, vol. 651, pp. 198-198–213, Jan. 2016, doi: 10.1016/j.msea.2015.10.068.

[6]   B. Zhang and H. Zirath, 'Metallic 3-D Printed Rectangular Waveguides for Millimeter-Wave Applications', *IEEE Trans. Compon. Packag. Manuf. Technol.*, vol. 6, no. 5, pp. 796–804, May 2016, doi: 10.1109/TCPMT.2016.2550483.

[7]   M. Awd, J. Tenkamp, M. Hirtler, S. Siddique, M. Bambach, and F. Walther, 'Comparison of Microstructure and Mechanical Properties of Scalmalloy® Produced by Selective Laser Melting and Laser Metal Deposition', *Materials*, vol. 11, no. 1, Art. no. 1, Jan. 2018, doi: 10.3390/ma11010017.

[8]   E. T. Jaynes, 'Ghost Modes in Imperfect Waveguides', *Proc. IRE*, vol. 46, no. 2, pp. 416–418, Feb. 1958, doi: 10.1109/JRPROC.1958.286913.

[9]   L. He, X. Zhong, Z. Fan, Q. Zhang, and W. Zhang, 'Evanescent-Mode Waveguide Filter with Transmission Zeroes Created by Shorted Waveguide Shunted in Coupling Region', in *Communications, Signal Processing, and Systems*, vol. 517, Q. Liang, X. Liu, Z. Na, W. Wang, J. Mu, and B. Zhang, Eds. Singapore: Springer Singapore, 2020, pp. 399–404. doi: 10.1007/978-981-13-6508-9_48.

[10]   P. Zhao and K. Wu, 'Waveguide Filters With Central-Post Resonators', *IEEE Microw. Wirel. Compon. Lett. Microw. Wirel. Compon. Lett. IEEE IEEE Microw Wirel. Compon Lett*, vol. 30, no. 7, pp. 657-657–660, Jul. 2020, doi: 10.1109/LMWC.2020.2995890.

[11]   D. M. Pozar, 'Microwave Engineering'. https://books.google.es/books?hl=es&lr=&id=_YEbGAXCcAMC&oi=fnd&pg=PA28&dq=+%22Microwave+Engineering%22&ots=1VQ6pdyKai&sig=Jk_Cl8gcs_xQcbCL9ujKzYytBbQ&redir_esc=y (accessed May 24, 2021).

[12]   J. Hirokawa and M. Ando, 'Single-layer feed waveguide consisting of posts for plane TEM wave excitation in parallel plates', *IEEE Trans. Antennas Propag. Antennas Propag. IEEE*

Trans. IEEE Trans Antennas Propagat, vol. 46, no. 5, pp. 625-625–630, May 1998, doi: 10.1109/8.668903.

[13]   R. E. Diaz and S. A. Clavijo, 'Artificial Magnetic Conductor', in *Encyclopedia of RF and Microwave Engineering*, K. Chang, Ed. Hoboken, NJ, USA: John Wiley & Sons, Inc., 2005, p. eme551. doi: 10.1002/0471654507.eme551.

[14]   A. Valero-Nogueira, E. Alfonso, J. I. Herranz, and P.-S. Kildal, 'Experimental Demonstration of Local Quasi-TEM Gap Modes in Single-Hard-Wall Waveguides', *IEEE Microw. Wirel. Compon. Lett. Microw. Wirel. Compon. Lett. IEEE IEEE Microw Wirel. Compon Lett*, vol. 19, no. 9, pp. 536-536–538, Sep. 2009, doi: 10.1109/LMWC.2009.2027051.

[15]   E. Pucci and P.-S. Kildal, 'Contactless non-leaking waveguide flange realized by bed of nails for millimeter wave applications', Mar. 2012, pp. 3533-3533–3536. doi: 10.1109/EuCAP.2012.6206199.

[16]   A. Valero-Nogueira and E. Alfonso, 'How gap waveguides were conceived', in *2017 11th European Conference on Antennas and Propagation (EUCAP)*, Paris, France, Mar. 2017, pp. 242–246. doi: 10.23919/EuCAP.2017.7928260.

[17]   A. Tamayo Domínguez, 'Advances in Periodic Structures and Manufacturing Technologies for mm-Wave Antennas', PhD Thesis, Universidad Politécnica de Madrid, 2020. doi: 10.20868/UPM.thesis.65851.

[18]   A. T. Dominguez, J. M. F. Gonzalez, J. M. I. Alonso, and M. Sierra-Perez, 'Design proposal for Ridge Gap Waveguide and comparison with other technologies in Ka to W bands', in *2016 10th European Conference on Antennas and Propagation (EuCAP)*, Davos, Switzerland, Apr. 2016, pp. 1–5. doi: 10.1109/EuCAP.2016.7481554.

[19]   'SLM-processed Sc- and Zr- modified Al-Mg alloy_ Mechanical properties and microstructural effects of heat treatment | Elsevier Enhanced Reader'. https://reader.elsevier.com/reader/sd/pii/S0921509317308559?token=D49321C06F612074C7A1A4A55EB1E036891B7BD5F0B14435E8446AE369FFEF9FA2DA96C87BDC19D3A5293DC323FAD6AC&originRegion=eu-west-1&originCreation=20210606155449 (accessed Jun. 06, 2021).

[20]   D. Koutny *et al.*, 'Processing of Al-Sc aluminum alloy using SLM technology', *Procedia CIRP*, vol. 74, pp. 44-44–48, Jan. 2018, doi: 10.1016/j.procir.2018.08.027.

[21]   R. J. Cameron, C. M. Kudsia, and R. R. Mansour, *Microwave Filters for Communication Systems : Fundamentals, Design, and Applications*. Somerset, UNITED STATES: John Wiley & Sons, Incorporated, 2018. [Online]. Available: http://ebookcentral.proquest.com/lib/upnasp-ebooks/detail.action?docID=5341518

[22]   A. Volkov, 'Phased Antenna Array Optimization using CST and Python', 2020, doi: 10.13140/RG.2.2.10627.53282.

[23]   J.-S. Hong and J.-S. Hong, *Microstrip Filters for RF / Microwave Applications*. Hoboken, UNITED STATES: John Wiley & Sons, Incorporated, 2011. Accessed: May 15, 2021. [Online]. Available: http://ebookcentral.proquest.com/lib/upnasp-ebooks/detail.action?docID=644868